Ocean Engineering 148 (2018) 312–330

Contents lists available at ScienceDirect

Ocean Engineering

journal homepage: www.elsevier.com/locate/oceaneng

Influence of ship dynamics modelling on the prediction of fishing vessels roll response in beam and longitudinal waves

Marcos Míguez González [a,*], Gabriele Bulian [b]

[a] Integrated Group for Engineering Research, University of A Coruña, Mendizábal s/n, 15403, Ferrol, Spain
[b] Department of Engineering and Architecture, University of Trieste, Via A. Valerio 10, 34127, Trieste, Italy

ARTICLE INFO

Keywords:
Fishing vessels
Stability
Parametric roll
Dead-ship condition
Safety

ABSTRACT

Fishing is one of the most risky occupations worldwide. Many accidents are due to stability failures, and dynamic stability phenomena in waves are among the possible causes. Due to time, cost and regulatory lacks, these phenomena are not addressed during design of fishing vessels. High fidelity six degrees of freedom (6-DOF) codes can cope with these phenomena, but their complexity, cost and time of application, limit their use to high-end vessels. The use of less demanding approaches appears more suited for the fishing sector. The scope of this paper is to compare a 6-DOF blended code, 1-DOF nonlinear roll models and simplified analytical formulae, in order to assess the level of dispersion of the obtained roll motion predictions among tools with different levels of complexity. The roll response for a medium-sized stern trawler is investigated in regular beam and longitudinal waves, at zero speed. Results from the simplified models are in fair agreement with those from the 6-DOF code, at least for moderate wave steepnesses. Simplified models could provide a valuable tool for the assessment of fishing vessels behaviour at the early design stage, considering also their ease of implementation within typical existing naval architecture software.

1. Introduction

Fishing sector is the one within the maritime industry with the largest fleet worldwide. The total number of engine powered fishing vessels is over 2.900.000 according to the latest FAO statistics (FAO, 2016a); 80% of these units are from Asian countries, 7% from Latin-American countries, 6% from African ones, 3% of this fleet belongs to Europe, another 3% to the U.S. and, finally, 1% to Oceania. One characteristic of the fishing fleet is its vast heterogeneity. Different regulatory frameworks, distance to the fishing ground, caught species, regional tradition or even meteorological characteristics of their area of operation, lead to many different designs, which make it difficult to categorize fishing vessels into a limited set of typologies.

However, a classification according to the ship length is usually done based on the applicability limits of the different IMO and FAO instruments. On the one hand, there are vessels of 24 m in length and over, which should be under the regulatory framework of the Torremolinos Protocol (IMO, 1993), the Cape Town Agreement (IMO, 2012), the Part B of the Code of Safety for Fishermen and Fishing Vessels (FAO/ILO/IMO, 2005a) and the 2008 Intact Stability Code (IMO, 2008a). On the other hand, there are medium sized fishing vessels with lengths between 12 m and over and up to 24 m, to which the Voluntary Guidelines for the Design, Construction and Equipment of Small Fishing Vessels (FAO/ILO/IMO, 2005b) are of application. And finally, there are small vessels of under 12 m length, which are within the scope of the Safety Recommendations for Decked Fishing Vessels of Less than 12 m in Length and Undecked Fishing Vessels (FAO/ILO/IMO, 2012). In addition, it has to be said that none of the previous international regulations regarding fishing vessel safety are nowadays of mandatory application; these vessels are only required to fulfil regional regulations or agreements, which are in fact quite variable depending on the flag state of the ship. According to this categorization, latest data (FAO, 2016a) show that most of the worldwide fleet (85% of the vessels) belongs to the under 12 m group, while 13% belongs to the group with length between 12 and 24 m, and only 2% of the fleet has a length of 24 m and over. This distribution fits quite well the distribution of the regional fleets, such as, for example, the E.U. one (E.U., 2016).

Regarding the economic importance of the sector, it employs more than 37 million direct workers worldwide (not including aquaculture or processing industries). From these, 29 million are from Southeast Asian countries, more than 280.000 are from the U.S. and 150.000 are from the E.U. Fishing influence is especially relevant in the less developed

* Corresponding author.
E-mail addresses: mmiguez@udc.es (M. Míguez González), gbulian@units.it (G. Bulian).

https://doi.org/10.1016/j.oceaneng.2017.11.032
Received 12 April 2017; Received in revised form 7 November 2017; Accepted 12 November 2017

countries, where primary sectors have a prevalent role. Globally, fish trade activities have grown in the last years, with exports rising from 72 billion dollars in 2004 to 148 billion dollars in 2014 and imports rising from 76 billion dollars in 2004 to 140 billion dollars in 2014. China is the top exporter (13%), while the U.S. is the top importer (14%). If the case of the E.U. is used as an example of the situation of fishing in the more developed countries, it could be seen that, although fishing does not have a great impact on the economics of a whole country, it can have a big impact in some regions, where the local economy can be really fishing–dependent. While the Gross Value Added (GVA) of fishing and aquaculture to the total Gross Domestic Product (GDP) of the E.U. is a 0.1% and in Spain this relationship is a 0.2%, in Galicia, one of this high – dependant areas in Spain, this value rises up to a 1.3%. Regarding employment, more than 25% of all the workers within fishing of the E.U. are from just certain high – dependant regions of Spain, Greece, Portugal and Italy. If the case of Galicia is again mentioned, it accounts for 7.5% of the E.U. workers, 5.2% of the ships, 8.8% of the GT's and 14.5% of the value of the total E.U. catches (E.U., 2016; FAO, 2016a, 2016b; Meixide Vecino, 2015).

Despite these facts, safety is still one of the biggest problems affecting fishing sector, and fishing is still considered as one of the most dangerous industrial sectors, not only in the developing economies, but also in the fully developed ones. FAO estimates in more than 24.000 the number of casualties per year which directly affect fishing worldwide (Gudmundsson, 2013). In the case of countries like the USA (BLS, 2014), UK (Roberts, 2010) or Spain (MESS, 2014), although this number is sensibly lower, fishing is placed among the activities with largest fatal incident rates. In Jensen et al. (2014), a review of figures and trends of fatal accident incidence rates for different European countries (Norway, Denmark, Iceland, UK and Poland), USA and Canada can be found, showing the aforementioned high casualty rates.

If data from Jensen et al. (2014) and those from other sources (CIAIM, 2014; Lincoln, 2010; MAIB, 2016) are analysed, it can be appreciated that a large percentage of the casualties occur in the small - medium range of the fleet (vessels under 24 m length), and that many of them are due to stability failures, capsizing or bad weather (large wave struck). These accidents usually lead to the complete loss of the vessel in a sudden and fast way, making it very difficult for the crew to save themselves (Mata-Álvarez-Santullano and Souto-Iglesias, 2014).

This high percentage of stability-related accidents in the small segment of the fleet could be explained by different reasons. One reason is to be associated with the human factor. Crews of medium-small fishing vessels lack the training that those of larger vessels have. Due to this fact, they are not usually able to determine the risk level of their ship in a given operational situation or to understand the, typically few, stability information they have onboard (Womack, 2001). As a result, the crew on fishing vessels often base their judgement criteria just on their subjective experience. This lack of awareness, together with some occasional factors, such as not ensuring the vessel weather tightness, or the overloading of the vessel, is a major cause of these types of accidents (Míguez González et al., 2012; Spitzer, 1999; Wolfson Unit, 2004).

An additional aspect is the regulatory framework. As it has been already mentioned, the international mandatory regulations applicable to vessels of over 24 m length (Torremolinos Protocol and Cape Town Agreement), have not entered into force yet and, with the exception of those countries which have ratified any of them, only regional regulations are of application. In the case of vessels under 24 m, no international requirements are mandatory and, again, flag states are responsible of establishing the regulatory framework (Francescutto, 2013; Gudmundsson, 2013). In some cases, especially in the under 24 m range, these regional requirements do not reach the same safety levels as those of the IMO instruments (Gudmundsson, 2013; Kaplan and Kite-Powell, 2000; Spitzer, 1999; Wolfson Unit, 2004).

A further factor affecting the low safety score of fishing vessels are the environmental conditions. Fishermen are usually forced to sail in very harsh weather conditions, as their incomes are fully-dependant on catches. Taking into account that, with the notable exception of the Icelandic approach (Viggosson, 2009), there is no regulation which determines which weather conditions a given fishing vessel is allowed to sail in as a function of her size or stability levels, crews of smaller vessels usually face relatively worse conditions than those of the larger vessels (Spitzer, 1999).

Compared to larger vessels, small and medium sized fishing vessels sail in relatively more severe weather conditions, which can induce large amplitude motions and other dynamic effects, particularly roll. In fact, roll motion can significantly contribute in deteriorating the operability of the vessel (Mata-Álvarez-Santullano and Souto-Iglesias, 2014; Tello et al., 2011) and is, among all ship degrees of freedom, the one which can mostly compromise its safety. Moreover, in addition to stability failures associated to static/quasi-static effects (e.g. Mantari et al. (2011)), nonlinear dynamic roll instabilities are known to be among the causes of accidents involving fishing vessels (Mata-Álvarez-Santullano and Souto-Iglesias, 2013).

The evaluation of merchant and naval vessel vulnerability to the aforementioned instabilities has traditionally been done by using experimental tests, complex mathematical tools or both of these alternatives, which turned out to be a quite expensive and long process. In the case of fishing vessels, especially the smaller ones, their design process is usually very limited, not only in cost, but also in time. This is partially associated with the fact that profit margins of this activity are very low (an average of a 6% from 2010 to 2013 in the E.U., 2016), and long design and construction periods limit the vessel profitability. In case of EU countries, in addition, the need to shorten the design and construction time is due to the fact that current regulations require the decommissioning of one vessel in order to build another one with the same tonnage (Mata-Álvarez-Santullano and Souto-Iglesias, 2013). These limitations in cost and time have made it very rare to have dynamic stability analysis carried out within design stages in the case of fishing vessels.

At the same time, however, the need for taking into account dynamic stability phenomena in waves has been already acknowledged by researchers and regulators, and different published recommendations to skippers try to provide some information about how to avoid, or at least reduce, the inception of such phenomena (DFOHS, 2014; Gudmundsson, 2009; IMO, 2008a; Wolfson Unit, 2004; Womack and Johnson, 2003). In order to take into account these phenomena within the IMO intact stability regulatory framework, the IMO Second Generation Intact Stability Criteria (SGISC) are under development (SDC 2/WP.4, 2015; SDC 3/WP.5, 2016; SDC 4/5/1, 2016; SDC 4/INF.4, 2016; SDC 4/WP.4, 2017). The SGISC framework considers five different possible failure modes: parametric roll resonance, dead ship condition, pure loss of stability, surf riding/broaching, and excessive accelerations (Francescutto, 2016). However, such new criteria are not planned to be applied to fishing vessels. Hence, the development of SGISC is not considering fishing vessels in the tuning of standards.

Still, the operational scheme of fishing vessels makes them potentially vulnerable to some of these phenomena. Typically, while reeling in, these vessels could spend a long time sailing at very low speeds, even at zero speed, in head (trawlers and purse seiners) or beam seas (longliners and purse seiners). This reduced speed condition also takes place during the periods when catches are processed after the recovery of the fishing gear and nets. In addition, they could also sail at slow speeds, in low manoeuvrability situations and with a catch-dependant heading (letting out purse seiners, letting out or trawling trawlers), or at moderate speeds with some more steering capabilities (as is the case of letting out longliners). This operational profile makes fishing vessels prone to experiencing parametric roll resonance in head seas or pure roll resonance in beam seas (equivalent to the dead ship condition considered in the SGISC). On a normal sailing at cruise speed, and as a consequence of the relatively small absolute dimensions, fishing vessels could also

experience pure loss of stability and surf-riding/broaching (Mata-Álvarez-Santullano and Souto-Iglesias, 2014; Míguez González et al., 2015; Perez Rojas et al., 2006). The operational requirements, which in some conditions reduce the possibility of modifying the speed or heading, make the potential vulnerability of fishing vessels to dynamic stability phenomena in waves, even higher. However, it is also worth highlighting that, in some of these situations, especially in the trawling condition, the effect of fishing nets on ship motions could be remarkable.

Nowadays, a variety of mathematical models exist for the prediction of the aforementioned dynamic stability phenomena, which can be considered to be potentially applicable at design stage. These go from the more complex and accurate nonlinear time domain 6 degrees of freedom (6-DOF) blended models, to the simplest nonlinear time domain 1 degree of freedom (1-DOF) ones. Blended (or hybrid) simulation models use different assumptions and approximations in order to arrive at practical simulation tools for nonlinear ship motions in waves, which balance accuracy and computational time. The scope of the approximations introduced in these tools is, basically, to embed the major forcing terms which drive nonlinear ship motions in waves, without exactly solving the fluid structure interaction problem in time domain. A number of examples of such tools can be found in literature, as mentioned also by Peters et al. (2012). Examples are FREDYN (de Kat and Paulling, 1989; McTaggart and de Kat, 2000), LAIDYN (Matusiak, 2007), LAMP (Liut et al., 2002; Shin et al., 2003; Spyrou et al., 2009), NMRIW (Ogawa, 2009), SHIXDOF (Bulian and Francescutto, 2013), TEMPEST (Belknap and Reed, 2010), and the tools developed by Ayaz et al. (2006), Greco and Lugni (2012, 2013), Grochowalski et al. (1998) and Liu and Papanikolaou (2016), among others. Blended tools, were also discussed by Beck and Reed (2001) and, more recently, in the review by Bačkalov et al. (2016).

In the case of parametric roll resonance, it is also well worth mentioning also 3-DOF models, which include the dynamic coupling effects of pitch and heave on roll motion, which are of paramount importance for the correct evaluation of the phenomenon (Munif and Umeda, 2006; Taguchi et al., 2011). An example of this alternative was presented by Neves and Rodríguez (2006), which has been applied to the evaluation of the behaviour of parametric roll in regular longitudinal waves for the case of fishing vessels (Neves and Rodríguez, 2009) and other cargo ships (Rodríguez et al., 2007). However, although 3-DOF models are far simpler than 6-DOF ones, they are still much more complex than the 1-DOF alternatives, as the number of parameters required for their setting up is much larger (and which include added mass, damping and excitation terms for heave, pitch and roll motions, together with coupling among them).

As a result from the above, 6-DOF can be considered to represent the state-of-the-art regarding nonlinear ship motion simulation with a view to application in ship design, while 1-DOF alternatives are characterised by a more tailored applicability to specific phenomena and an expected reduced accuracy compared to more complex models. 3-DOF models are herein considered to be as a too complex option for vulnerability assessment at design stage of fishing vessels. An extensive review in this respect has recently been given by Bačkalov et al. (2016), where a detailed analysis of most of the available alternatives can be found.

In some cases, 1-DOF models can also be further simplified by developing specific analytical formulae, which might partially avoid the necessity of going through time domain simulations. It is also worth noting that this mentioned range of modelling correspond to that embedded within the SGISC framework at different assessment levels.

From the above discussion, considering the fast&cheap requirements implicit within the fishing vessel design sector, it is evident that 1-DOF (or even simpler) roll models likely represent the most practically feasible option for the assessment of possible vulnerability of a fishing vessel to potentially dangerous dynamic stability phenomena in waves. Proposals in this respect were already put forward in the past by, e.g., Bulian and Francescutto (2006). It is however known that reduced-DOF models have limitations induced by their inherent simplifications. In this context, it is therefore important to investigate how the predictions from simplified models compare with those from higher fidelity tools, in order to verify whether the two approaches provide vulnerability indications which are sufficiently in line for an application of simplified models as a design tool.

This is, in fact, the problem addressed by the paper, i.e. a comparative investigation among models with different levels of complexity. In the past, conceptually similar investigations were carried out by Munif and Umeda (2006), who compared a 1-DOF model for parametric roll with a 6-DOF model with linearized heave and pitch for an Icelandic trawler in a small set of longitudinal regular waves at zero speed, and by Somayajula and Falzarano (2017), who compared the results from a 6-DOF tool with those obtained by different simplified 1-DOF models for the case of parametric rolling in irregular waves for a C11 containership. Also Bulian et al. (2012) compared predictions from simplified 1-DOF nonlinear roll models with those obtained from the same 6-DOF tool used herein, for a Series 60 hull form, but for the case of bi-chromatic beam waves at zero speed.

This paper focuses on fishing vessels and addresses parametric roll 2:1 subharmonic resonance in longitudinal regular waves and 1:1 roll resonance in beam regular sea waves, at zero speed, considering a wide range of wave conditions. Results from a high fidelity 6-DOF blended model (Bulian and Francescutto, 2013; Bulian et al., 2012, 2015, 2016; Cercos-Pita et al., 2016; Moro et al., 2015), which has the main characteristics for application at the envisioned Direct Stability Assessment Level of IMO Second Generation Intact Stability Criteria (SLF 52/WP.1-Annex 2, 2010; Annex 1 in SDC 4/WP.4, 2017), are compared with outcomes from simpler 1-DOF nonlinear roll models for the two considered conditions (Bulian, 2006; Bulian and Francescutto, 2006; Bulian et al., 2012). Predictions based on simplified approximate prediction formulae derived from the proposed 1-DOF roll models are also considered. For the analysis, a mid-sized stern trawler, which could be considered to be representative of the Spanish fishing fleet, has been selected. It is recognised that, in principle, the effect of nets should also be taken into account for the prediction of actual fishing vessel behaviour at sea. However, herein the focus is on the relative comparison between the different types of dynamical models in nominal regular waves. As a result, the inclusion of effects of nets on ship motions has not been considered. It is also underlined that including such effects is associated with a significant complexity, with clear difficulties in the introduction of such effects, particularly, in the 1-DOF models.

The paper is structured as follows. First, the mathematical models used in the comparative study, are presented, together with the simplified approximate formulae derived from the 1-DOF models. Next, the numerical experiments that have been carried out are described. This section provides a description of the characteristics of the considered fishing vessel, the description of the tests and the analysis of the obtained results. Roll motion amplitude is reported for different regular wave steepnesses and frequencies, in head and beam seas and zero speed, using the different considered approaches. Finally, some conclusions regarding the possible applicability of the considered simplified models at the vessel design stage, are reported.

2. Description of mathematical models

2.1. 1-DOF models

1-DOF nonlinear models used in this study for the analysis of roll behaviour in case of 1:1 resonance in regular beam waves and in case of 2:1 parametric roll resonance in longitudinal regular waves, are typical 1-DOF models employed in the field of nonlinear roll motion dynamics (see, e.g., Belenky and Sevastianov (2007) or Bačkalov et al. (2016) and references therein). Each model, however, will be studied in two variants, as described in details in the following sections. Moreover, for each model, a simplified analytical formulation for the determination of an

approximate maximum roll response will also be provided. In this respect, considering the target of the study, the simplified formulae will be considered at the maximum possible level of simplification.

In the present work, two different alternatives for the simple 1-DOF model have been studied in both the head and beam sea cases. In the head seas case, a nonlinear model of roll motion, based on the look-up-table approach for obtaining the *GZ* in waves has been selected, considering the vessel both as free to trim in waves in the computations of *GZ*, or with a fixed constant trim. In the case of beam waves, two options have been applied for implementing the wave excitation within the model: the "absolute angle model", which considers wave moments as an external excitation term which is separate from the restoring term, and the "relative angle model", where wave excitation is included within the nonlinear restoring term. It is underlined that both models considered herein describe the dynamics of the absolute roll angle, and the wordings "absolute" and "relative" are meant to identify the type of approach which is used for the modelling of the moment exerted on the inclined vessel in presence of waves.

2.1.1. Beam waves

In this work, two different 1-DOF models are considered for analysing the roll motion response in regular beam waves. In both cases, the inherent nonlinearities of large amplitude roll motion are taken into account through nonlinear restoring and nonlinear damping terms.

The first model, is the most frequently used 1-DOF nonlinear roll model for describing the absolute roll angle ϕ in the beam sea condition (Bulian and Francescutto, 2006; Francescutto and Contento, 1999; Spyrou et al., 2002; Wu and McCue, 2008, among others, and see also references in Bačkalov et al. (2016)):

$$\ddot{\phi} + 2\cdot\nu\cdot\omega_0\cdot\dot{\phi} + \beta\cdot\dot{\phi}\cdot|\dot{\phi}| + \delta\cdot\dot{\phi}^3 + \omega_0^2\cdot\frac{GZ(\phi)}{GM_T} = \omega_0^2\cdot\alpha_{eff}(t) \tag{1}$$

In this model, the righting lever curve in still water, as a function of the absolute roll angle, $GZ(\phi)$, is considered in the nonlinear restoring term, and roll damping comprises linear and nonlinear terms (coefficients ν, β and δ). The calm water metacentric height is indicated as GM_T, while ω_0 is the roll natural frequency. It is noted that the wave excitation term appears on the right hand side of the equation as a separate term with respect to the restoring which appears on the left hand side. In the excitation term, the wave moment is implemented using the "effective wave slope" (α_{eff}) approach, as follows:

$$\alpha_{eff}(t) = \pi\cdot r\cdot s_w\cdot\cos(\omega_e\cdot t + \psi) \tag{2}$$

where s_w is the wave steepness, ω_e is the encounter wave frequency, ψ is a generic phase, and r is the effective wave slope coefficient. In case drifting is not explicitly accounted for, the encounter wave frequency corresponds to the physical wave frequency. Moreover, the phase ψ can be taken as zero considering an appropriate translation of the origin of time. The effective wave slope coefficient is assumed to depend on the ship geometry and on considered wave. It is worth underlining that modelling of the type in (1)–(2) has been accepted by the IMO in the framework of the alternative assessment of weather criterion on an experimental basis, through MSC.1/Circ.1200 (Francescutto et al., 2004; IMO, 2006). In particular, MSC.1/Circ.1200 allows using a Parameter Identification Technique (PIT), based on a modelling of the type (1)–(2), where the model parameters are determined from model scale experiments in beam waves, and the 1-DOF model is then used to predict roll motion in the required conditions for the Weather Criterion.

The absolute angle model, however, has been shown to present some consistency issues (Bulian and Francescutto, 2009, 2011), and a thinking to the actual physics of the fluid structure interaction would suggest that a model accounting for a (corrected) relative angle between the ship and the wave could be more appropriate.

As second model, therefore, the partially relative angle approach from Bulian and Francescutto (2009, 2011) is applied, where the wave excitation is included within the restoring term. This alternative, which can be referred to as "effective relative angle" approach, still describes the dynamics of the absolute roll angle ϕ as the previous "absolute angle approach". However, in contrast to the previous model, it tries to take into account the effect of relative angle between the ship and the wave for the computation of fluid-structure interaction moment. More precisely, this alternative tries to take into account the fact that, differently from the linear case, in a nonlinear framework it is not possible to separate the "restoring" from the "wave excitation", since these two effects are both included in the moment exerted on the vessel due to the total pressure on the hull. This second 1-DOF alternative for the beam sea condition takes the following form:

$$\ddot{\phi} + 2\cdot\nu\cdot\omega_0\cdot\dot{\phi} + \beta\cdot\dot{\phi}\cdot|\dot{\phi}| + \delta\cdot\dot{\phi}^3 + \omega_0^2\cdot\frac{GZ\left(\phi - \alpha_{eff}(t)\right)}{GM_T} = 0 \tag{3}$$

It can be noted that, as anticipated, the equation still describes the dynamics of the absolute roll angle ϕ. However, now, the instantaneous effective wave slope $\alpha_{eff}(t)$ is embedded in the calm water restoring, using the idea of the "effective relative angle" $\phi - \alpha_{eff}$. It is noted that when the roll restoring is linear, i.e. $GZ(\xi) = GM_T\cdot\xi$, or when the angle for the calculation of the restoring is small enough, i.e. $GZ(\xi) \approx GM_T\cdot\xi$, then the two models (1) and (3) reduce to the same model.

Historically, the idea of describing roll motion dynamics using a reasoning based on the concept of relative angle can be dated back to Froude (1861), who used a long wave approximation (i.e. $r = 1$) and a linear restoring. However, in the literature it is possible to find different approaches based on the relative angle modelling. For instance, Wellicome (1975) and Wright and Marshfield (1980) used an approach where all terms in the dynamic equation (added inertia, damping, restoring combined with forcing) are based on the relative angle $\phi - \alpha$ (and appropriate corresponding derivatives), neglecting the effective wave slope coefficient under the assumption of long waves, and they considered nonlinear damping and nonlinear restoring. Instead, Tamiya (1975), for instance, used a mathematical model where the added inertia and the damping terms are based, respectively, on the first and on the second derivative of the absolute roll angle. The restoring and excitation are combined using a corrected restoring lever of the type $r\cdot GZ(\phi - \alpha)$, i.e. using the nominal relative angle between the ship and the wave $\phi - \alpha$, and using the effective wave slope as a global corrective multiplicative factor. Moreover, eventually, also Tamiya (1975) used the long wave approximation, assuming $r = 1$. These mentioned models differ from (3), since, in the model presented herein, the added inertia and the damping term are based on the absolute roll angle (like Tamiya (1975)), but the restoring plus forcing term $GZ(\phi - r\cdot\alpha)$ is based on an "effective relative angle", where the effective wave slope is used as a correction factor only for the wave slope. Specific discussions regarding the use of absolute versus relative angle for the modelling of roll motion have been provided by Belenky and Sevastianov (2007) and by Bulian and Francescutto (2011).

The frequency dependent effective wave slope coefficient (r), which is included in the forcing term in both models, can be predicted by using different methodologies. One approach for its computation is based on a decoupling of the linear hydrodynamics seakeeping equations (Bulian and Francescutto, 2009, 2011; Naciri and Lledo, 2001). A second, simpler approach, which does not require the hydrodynamic solution of the fluid-structure interaction problem, is based on the determination of r by direct computation of roll moment induced by the Froude-Krylov forces with respect to the vessel centre of gravity (e.g. Umeda and Tsukamoto (2008)). Finally, two simplified semi-empirical methods exist, as proposed by (Blume, 1979) and as available in the IMO Weather Criterion (IMO, 2008a). In these two latter cases, however, the effective wave slope is provided only for a value of wave frequency corresponding to the vessel natural roll frequency. In this work, although some comparisons will be provided considering the four mentioned alternatives, only the

first approach has been selected for the time domain calculations and comparisons with results from the 6-DOF model.

For both models (1) and (3), an approximate solution for the maximum roll amplitude can be obtained by means of a straightforward simplified analytical approach, if nonlinearities in damping are retained, but those in restoring are neglected. In this case, the maximum expected roll amplitude for a given wave of steepness s_W and a given effective wave slope coefficient r, can be obtained by solving the following equation for the roll amplitude A_{roll}:

$$A_{roll} = \frac{\pi \cdot r \cdot s_W}{2 \cdot \nu_e(A_{roll})} \tag{4}$$

where $\nu_e(A_{roll})$ is the dimensionless linear equivalent roll damping coefficient at the roll natural frequency, and it can be calculated as (Himeno, 1981; Ikeda et al., 1978):

$$\nu_e(A_{roll}) = \nu + \frac{4}{3 \cdot \pi} \cdot \beta \cdot A_{roll} + \frac{3}{8} \cdot (\delta \cdot \omega_0) \cdot A_{roll}^2 \tag{5}$$

The combination of (4) and (5) leads to a polynomial equation for A_{roll} which, in general, can be solved through simple numerical methods. It is also worth mentioning that the formula for the roll amplitude in the present Weather Criterion (IMO, 2008a), basically corresponds to what is obtained from (4) and (5) when only a pure quadratic damping is considered. However, the formula in the Weather Criterion also contains a semi-empirical 30% reduction in roll amplitude with respect to that which would be observed in regular beam waves (see IMO (2006, 2008b)).

For the considered fishing vessel, results from the two mentioned 1-DOF models, as well as results from the simplified approach (4)/(5), will be compared with outcomes from the 6-DOF model which will be described later.

2.1.2. Longitudinal waves

The 1-DOF model considered herein for the analysis of parametrically excited roll motion response in regular longitudinal waves is what can be considered to be the most commonly used simplified model. Similarly to the beam sea case, inherent nonlinearities of large amplitude roll motion, which are of paramount importance to accurately compute the rolling amplitude, are taken into account through nonlinear restoring and nonlinear damping terms. In this case, nonlinear roll restoring is calculated as a function of both the heeling angle and of the wave crest position in time along the hull.

The used 1-DOF non-linear roll model takes the following form:

$$\ddot{\phi} + 2 \cdot \nu \cdot \omega_0 \cdot \dot{\phi} + \beta \cdot \dot{\phi} \cdot |\dot{\phi}| + \delta \cdot \dot{\phi}^3 + \omega_0^2 \cdot \frac{GZ(\phi, t)}{GM_T} = 0 \tag{6}$$

where, as in (4), ν, β and δ are linear and nonlinear damping coefficients, ω_0 is the natural roll frequency of the ship, GM_T is the still water metacentric height, but now $GZ(\phi, t)$ is the time varying nonlinear heeling lever as a function of roll angle and time, and it depends on the wave length and steepness considered in the simulation. Regarding damping, it is here underlined that the linear term is dominant at small rolling amplitudes and it governs, together with the variation of the linear term of $GZ(\phi, t)$ (i.e. $GM_T(t)$), the parametric roll inception boundary. On the other hand, nonlinearities of damping and restoring affect large amplitude motions.

The 1-DOF model in (6) has been used in the past for different types of vessels (see, e.g., references in Bačkalov et al. (2016)) including also fishing vessels (Bulian and Francescutto, 2006; Munif and Umeda, 2006). Moreover, this type of model has been also adopted in class rules as a sufficient tool for addressing the vessel vulnerability to parametric roll (ABS, 2004) and it has been used in the development of parametric roll vulnerability criteria in IMO SGISC, in particular at Level 2-Check 2 vulnerability assessment (SDC 3/WP.5, 2016; Tompuri et al., 2014).

The time, wave and roll angle dependent restoring term, the $GZ(\phi, t)$, is computed by using a standard hydrostatic software, under the quasi-static assumption. To this end, two different approaches have been considered: one where the vessel is free to trim and sink, as a function of the wave crest position and heel (fixed-trim approach); and another alternative where the vessel trim is fixed, while letting the sinkage free (free-trim approach). This model considers that the equilibrium of the vessel is obtained in a quasi-static way. Although this approach misses the dynamic effects of heave and pitch, it has shown to provide reasonably accurate results in various cases (Bulian, 2006).

Similarly to the case of 1:1 resonance in beam regular waves, also in case of 2:1 subharmonic resonance in longitudinal regular waves a simplified expression for the maximum amplitude of parametrically excited roll motion (A_{roll}) can be obtained if the restoring is approximated to be linear, and if only nonlinearities in damping are retained. To this end, first, the amplitude of parametric excitation is defined as:

$$h_0 = \frac{\delta GM_T}{GM_T} = \frac{f_1 \cdot \lambda_W \cdot s_W}{2 \cdot GM_T} \tag{7}$$

where λ_W and s_W are, respectively, the length and steepness of the considered wave, δGM_T is the variation of vertical position of metacentre for the considered wave and f_1 is the coefficient playing the role of an (approximate) transfer function of GM_T variation in waves, similar to that proposed by (Dunwoody, 1989). Then, if the condition of frequency of encounter equal twice the natural roll frequency is fulfilled for the considered wave, the maximum amplitude of parametrically excited roll motion (A_{roll}) can be obtained by solving the following equation

$$h_0 = 4 \cdot \nu_e(A_{roll}) \tag{8}$$

where $\nu_e(A_{roll})$ is the dimensionless linear equivalent roll damping coefficient in (5). Also in this case, the combination of (8) and (5) leads to a polynomial equation for A_{roll} which, in general, can be solved through simple numerical methods. Equation (8) can be obtained as a simplification of the more general approximate expressions in (Bulian, 2004). Moreover, the same type of simplified expression has been considered in the development of Level 1 vulnerability assessment criteria for parametric roll in SGISC (SDC 4/5/1, 2016). It shall be noted, however, that the approximation (8) does not account for the effect of nonlinear restoring which, in case of parametrically excited roll motion, can be significant. Formulations involving nonlinear restoring, at different levels of approximations, and, depending on cases, with or without nonlinear damping, can be found in Bulian (2004), ITTC (2006) and SDC 4/5/1 (2016).

2.2. 6-DOF blended code

Direct nonlinear analysis of fluid structure interaction through CFD codes with moving/overlapping meshes, presently represents the most advanced approach for simulation of ship motions in waves (e.g. Sadat-Hosseini et al., 2010). However, as outlined by Bačkalov et al. (2016), such tools are still too time consuming for a systematic application, such as that which is required in the framework of ship design, where a large number of different scenarios need to be investigated. As a result, in the framework of nonlinear ship motions simulations, the state-of-the-art are the so-called hybrid (or blended) 6-DOF models, which are considered to represent reference high-fidelity tools. The aim of these tools is the simulation of nonlinear motions of a vessel, possibly manoeuvring and self-propelled, in waves, taking into account the main sources of nonlinearities which could cause dangerous dynamic stability phenomena in waves. The model underlying such simulation codes typically blends linear hydrodynamics, nonlinear Froude-Krylov effects, semi-empirical models for manoeuvring, additional roll damping dissipation terms, semi-empirical models for wind loads, etc. Hybrid models have been considered to represent a potentially viable tool for the so-called Direct

Stability Assessment level and for the development of ship-specific Operational Guidance, in the framework of IMO Second Generation Intact Stability Criteria (SLF 52/WP.1-Annex 2, 2010; Annex 1 in SDC 4/WP.4, 2017). As anticipated also in the introduction of the paper, due to the partial semi-empiricism which is inherent in hybrid models, different implementation variants are available in literature (e.g. Ayaz et al., 2006; Belknap and Reed, 2010; Bulian and Francescutto, 2013; de Kat and Paulling, 1989; Greco and Lugni, 2012, 2013; Grochowalski et al., 1998; Liu and Papanikolaou, 2016; Liut et al., 2002; Matusiak, 2007; McTaggart and de Kat, 2000; Ogawa, 2009; Shin et al., 2003; Spyrou et al., 2009). Recent developments in this respect are reported by Bačkalov et al. (2016).

The 6-DOF model used herein is SHIXDOF (Bulian and Francescutto, 2013; Bulian et al., 2012, 2015, 2016; Cercos-Pita et al., 2016; Moro et al., 2015). SHIXDOF integrates the 6-DOF nonlinear rigid body equations of motions, projected, as usual, to the ship-fixed reference system, under the effect of "external" forces:

$$
\begin{cases}
m\cdot[\mathbf{u_O}\prime+\boldsymbol{\omega}\wedge\mathbf{u_O}+\boldsymbol{\omega}\prime\wedge\mathbf{x_G}+\boldsymbol{\omega}\wedge(\boldsymbol{\omega}\wedge\mathbf{x_G})]=\mathbf{F_{ext}}(t)\\
\mathbf{I_O}\cdot\boldsymbol{\omega}\prime+\boldsymbol{\omega}\wedge(\mathbf{I_O}\cdot\boldsymbol{\omega})+m\cdot\mathbf{x_G}\wedge\mathbf{u_O}\prime+m\cdot\mathbf{x}_G\wedge(\boldsymbol{\omega}\wedge\mathbf{u_O})=\mathbf{M}_{\mathbf{ext},O}(t)\\
\\
\dfrac{d\boldsymbol{\xi}_\mathbf{O}}{dt}=\underset{\mathbf{S}\to\boldsymbol{\Sigma}}{\mathbf{R}}\cdot\mathbf{u_O}=\\
=\begin{pmatrix}\cos(\psi)&-\sin(\psi)&0\\ \sin(\psi)&\cos(\psi)&0\\ 0&0&1\end{pmatrix}\cdot\begin{pmatrix}\cos(\vartheta)&0&\sin(\vartheta)\\ 0&1&0\\ -\sin(\vartheta)&0&\cos(\vartheta)\end{pmatrix}\cdot\begin{pmatrix}1&0&0\\ 0&\cos(\phi)&-\sin(\phi)\\ 0&\sin(\phi)&\cos(\phi)\end{pmatrix}\cdot\mathbf{u_O}\\
\dfrac{d\boldsymbol{\varepsilon}}{dt}=\begin{pmatrix}1&\sin(\phi)\cdot\tan(\vartheta)&\cos(\phi)\cdot\tan(\vartheta)\\ 0&\cos(\phi)&-\sin(\phi)\\ 0&\sin(\phi)/\cos(\vartheta)&\cos(\phi)/\cos(\vartheta)\end{pmatrix}\cdot\boldsymbol{\omega}
\end{cases}
\tag{9}
$$

In (9) vectors and matrices are reported in bold, and primes indicate time derivatives carried out in the ship-fixed reference system. The first two equations are the equations of 6-DOF nonlinear rigid body dynamics projected in the ship-fixed reference system, and, therefore, all involved vectors are considered to be represented in such reference system. The ship-fixed reference system is right handed and it has the x-axis longitudinal (directed from stern to bow), the y-axis transversal (directed from starboard to port side) and the z-axis vertical (directed upwards, from bottom to top). m is the mass of the ship, the vector $\mathbf{u_O}=(u,v,w)^T$ is the speed vector of the chosen centre O of the ship-fixed reference system for the simulations, $\boldsymbol{\omega}=(p,q,r)^T$ is the rigid body angular velocity, $\mathbf{x_G}=(x_G,y_G,z_G)^T$ is the position vector of the centre of gravity G, $\mathbf{I_O}$ is the tensor of inertia with respect to O. External actions on the ship at the generic time t are represented by the force vector $\mathbf{F_{ext}}(t)=(F_{ext,x}(t),F_{ext,y}(t),F_{ext,z}(t))^T$ and the moment (w.r.t. O) vector $\mathbf{M}_{\mathbf{ext},O}(t)=(M_{ext,O,x}(t),M_{ext,O,y}(t),M_{ext,O,z}(t))^T$. Such external actions comprise the fluid-structure interaction, the possible effect of wind, propellers, restrain systems, etc. As usual, the first two equations representing rigid body dynamics are supplemented by the third and fourth equations in order to properly position and orient the vessel in the earth-fixed reference system at each time instant. The third equation, which allows translating the vessel in the earth-fixed reference system, represents the relation between the speed $\mathbf{u_O}$ expressed in components with respect to the ship-fixed reference system, and the time derivative of the position vector $\boldsymbol{\xi}_\mathbf{O}=(\xi_O,\eta_O,\zeta_O)^T$ of the point O expressed in the earth-fixed reference system. The matrix $\underset{\mathbf{S}\to\boldsymbol{\Sigma}}{\mathbf{R}}$, which depends on the Euler angles of roll (ϕ), pitch (ϑ) and yaw (ψ), is the transformation matrix from the ship-fixed to the earth-fixed reference system. Finally, the fourth equation links the angular velocity $\boldsymbol{\omega}$ expressed in components with respect to the ship-fixed reference system, to the time derivative of the vector of Euler angles, $\boldsymbol{\varepsilon}=(\phi,\vartheta,\psi)^T$, and it allows to properly orient the vessel in the earth fixed reference system. The convention used for the order of the Euler angles is the classical one used in Naval Architecture, namely first yaw, then pitch and finally roll.

With specific reference to the target of the present study, a description is given in the following of the modelling for the most relevant actions.

Froude-Krylov force and moment are determined by direct pressure integration on the instantaneous wetted hull (based on the undisturbed wave profile) $S_H(t)$, i.e.

$$
\begin{cases}
\mathbf{F_{FK}}(t)=\iint\limits_{S_H(t)}-p_T(\mathbf{x},t)\cdot\mathbf{n}(\mathbf{x})dS\\
\mathbf{M}_{\mathbf{FK},O}(t)=\iint\limits_{S_H(t)}\mathbf{x}\wedge(-p_T(\mathbf{x},t)\cdot\mathbf{n}(\mathbf{x}))dS
\end{cases}
\tag{10}
$$

where $p_T(\underline{x},t)$ is the total instantaneous undisturbed wave pressure, comprising also the hydrostatic term, and $\mathbf{n}(\mathbf{x})$ is the local outward normal vector. The total pressure is based on Airy linear theory. However, in order to guarantee zero pressure at the free surface, a stretching technique is applied to the linear field (Matusiak, 2010; Wheeler, 1969). The integration is numerically carried out using a discretisation of the hull in triangular panels.

Forces associated to the linear hydrodynamic modelling are split into two parts, namely radiation and diffraction (scattering). Radiation forces are determined, instantaneously, by means of convolution integrals using memory functions (Cummins, 1962) derived from linear hydrodynamic pre-calculations, and, herein, the implementation is as follows:

$$
\begin{cases}
\begin{pmatrix}\mathbf{F_{rad}}(t)\\ \mathbf{M}_{\mathbf{rad},O}(t)\end{pmatrix}=-\mathbf{A}_{\infty,O}\cdot\mathbf{h}\prime-\int_0^t\mathbf{K_O}(t-\tau)\cdot\mathbf{h}(\tau)d\tau\\
\mathbf{K_O}(\tau)=\dfrac{2}{\pi}\int_0^\infty\mathbf{B_O}(\omega)\cos(\omega\cdot\tau)d\omega\\
\mathbf{h}=\begin{pmatrix}\mathbf{u_O}\\ \boldsymbol{\omega}\end{pmatrix}
\end{cases}
\tag{11}
$$

In (11), $\mathbf{A}_{\infty,O}$ and $\mathbf{B_O}(\omega)$ are, respectively, the 6 × 6 matrices of infinite frequency added masses and frequency dependent damping, both with respect to the point O, while $\mathbf{K_O}(\tau)$ is the 6 × 6 matrix of memory functions depending on the time lag τ . Also the diffraction (scattering) force $\mathbf{F_{dif}}(t)$ and moment $\mathbf{M_{dif,O}}(t)$ with respect to O are based on linear hydrodynamic frequency domain pre-computations, and they are determined, at each time instant of the simulation, by making direct use of the force/moment transfer functions. In particular, at each time instant, the heading of the vessel with respect to the wave and the relative position of the vessel (point O) with respect to the wave crest, are determined. From these two variables, the instantaneous diffraction force and moment with respect to the point O, are obtained using the amplitude and phase information from the available pre-computed database of diffraction forces. Hydrodynamic coefficients $\mathbf{A}_{\infty,O}$ and $\mathbf{B_O}(\omega)$, as well as transfer functions of diffraction forces, are calculated for zero speed.

Drag effects are modelled by means of a cross-flow approach based on the local relative lateral speed between the vessel (accounting for nonlinear rigid body motions) and the undisturbed wave particles' velocity field (with stretching). Examples of approaches for modelling cross-flow, with specific attention to large amplitude ship motions in waves, have been described in the past by de Kat and Paulling (1989), Grochowalski et al. (1998) and Hughes et al. (2011). In the present tool, the force and moment due to cross-flow effects are obtained, at each time instant, by integration of local contributions on the instantaneous portion of the ship centreplane which is below water (considering the undisturbed wave profile), $S_{CP}(t)$:

$$\begin{cases} \mathbf{F_{drag}}(t) = \int\limits_{S_{CP}(t)} \frac{1}{2}\cdot\rho_{water}\cdot C_D(\mathbf{x})\cdot u_{rel-w,y}(\mathbf{x})\left|u_{rel-w,y}(\mathbf{x})\right|\cdot\hat{\mathbf{y}}\ dS \\ \mathbf{M_{drag,O}}(t) = \int\limits_{S_{CP}(t)} \mathbf{x}\wedge\left(\frac{1}{2}\cdot\rho_{water}\cdot C_D(\mathbf{x})\cdot u_{rel-w,y}(\mathbf{x})\left|u_{rel-w,y}(\underline{x})\right|\cdot\hat{\mathbf{y}}\right)\ dS \end{cases} \tag{12}$$

In (12), $C_D(\mathbf{x})$ is the local drag coefficient at the point $\mathbf{x}$ on the centreplane, $u_{rel-w,y}(\mathbf{x})$ is the local component along the ship-fixed y-axis of the relative velocity of water with respect to the vessel, and $\hat{\mathbf{y}}$ is the versor of the y-axis. The local relative speed accounts for the effect of the wave velocity field. When $C_D(\mathbf{x})$ on the ship centreplane does not depend on the vertical (ship-fixed) coordinate, the model reduces to a sectional cross-flow model. For the numerical determination of drag force and moment, the centreplane of the vessel is discretised into small panels, and, for each panel, the local contribution to the drag force and moment are determined, and eventually summed up.

Semi-empirical nonlinear roll damping contributions can also be added, and actually, in general, they need to be added, in order to tune the model with respect to roll dissipation. While, in principle, any general functional form can be used, the following one is typically applied for tuning purposes:

$$\mathbf{M_{add}}_{-damp,O}(t) = \left(-B_{44L,add,O}\cdot p - B_{44Q,add,O}\cdot p|p| - B_{44C,add,O}\cdot p^3\right)\cdot\hat{\mathbf{x}} \tag{13}$$

In (13), $\hat{\mathbf{x}}$ is the versor of the longitudinal ship axis and $B_{44L,add,O}$, $B_{44Q,add,O}$ and $B_{44C,add,O}$, are, respectively, linear, quadratic and cubic additional roll damping coefficients.

Additional forces, which are however less relevant for the cases addressed in this study, are also present in the modelling, as described by Bulian and Francescutto (2013) and Bulian et al. (2012, 2016).

3. Numerical experiments

Numerical experiments have been carried out on a sample vessel in the two considered conditions (beam and longitudinal regular waves) at zero speed. In longitudinal waves, the head sea condition has been considered. The mentioned models have been used and compared with the intention of analysing the level of agreement between predictions from the 6-DOF modelling and from the 1-DOF modelling.

3.1. Sample ship

The selected ship is a Spanish medium sized stern trawler, sailing in the Great Sole Bank area in southern Ireland. It is a two decked vessel, with a stern ramp for letting out and reeling in the nets.

The Spanish medium sized trawling fleet is composed of vessels sailing both in Spanish Atlantic grounds and in E.U. grounds in Irish and U.K. waters (Great Sole bank area). In both cases, vessels are similar in size and arrangement, being the latter slightly larger vessels. According to the latest (2016) Spanish fishing fleet statistics published by the Spanish Ministry of Agriculture and Fishing (MAPAMA, 2017), the

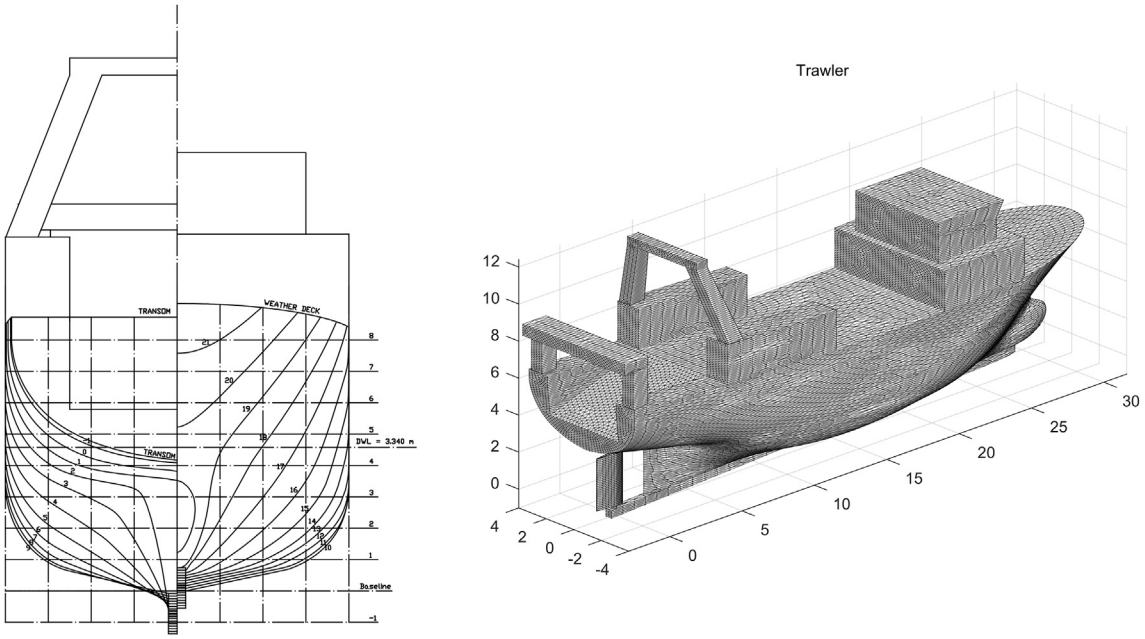

Fig. 1. Hull bodyplan (left) and 3D view of the mesh used in the 6-DOF simulations (right).

Table 1
Geometrical and mechanical data of the fishing vessel.

		Volume	448.0 m^3
Overall Length	34.50 m	Draught	3.340 m
Length between perpendiculars	29.00 m	Downflooding Angle	63.4°
Breadth	8.00 m	Metacentric height	0.350 m
Depth to Main Deck	3.65 m	Natural roll frequency	0.563 rad/s
Depth to Upper Deck	5.80 m	Dry roll radius of gyration (w.r.t. CoG)	3.0 m (38% B)
Design Draught	3.60 m	Dry pitch radius of gyration (w.r.t. CoG)	7.0 m (24% L_{bp})
		Dry yaw radius of gyration (w.r.t. CoG)	7.0 m (24% L_{bp})

Spanish trawling coastal fleet (sailing in Atlantic waters), is composed of 80 vessels, with an average overall length of 28.29 m and an overage Gross Tonnage of 227.3 GT. In the case of the Spanish trawling fleet operating in E.U. grounds (Great Sole bank), there are 55 vessels, with an average overall length of 32.68 m and an overage Gross Tonnage of 295.8 GT. Considering that the vessel selected in this work has an overall length of 34.50 m and a Gross Tonnage of 332 GT, and although it is on the upper range of overall length and Gross Tonnage values, it could be said that it adequately represents the Spanish mid-sized trawling fleet.

The typical operation of these vessels include cruising to and from the fishing area and letting out the nets, trawling and reeling in at slow speeds (no more than 3 to 4 knots). Headings usually only depend on maximising the amount of possible catches, trying to limit weathervaning only to very severe weather conditions. This fact makes these vessels potentially prone to experience 2:1 parametric roll resonance in head seas, and large roll motions due to 1:1 resonance in beam seas, at near zero speeds, due to the limited possibility of corrective actions.

In order to set up the mesh needed for the 6-DOF model, a 3D model of the vessel was prepared. For the sake of better resemblance to the real vessel, the rudder and the different superstructures were also included in the geometrical model. The vessel bodyplan, together with a view of the 3D model, are presented in Fig. 1.

The main characteristics of the vessel and the studied loading condition are presented in Table 1. The draught under analysis is obtained as a mean of the operational draught range of the vessel, while metacentric height was set to the minimum required value (350 mm) according to (IMO, 1993, 2008a). Fig. 2 shows the still water righting lever curve for the loading condition under analysis, computed under the free to trim

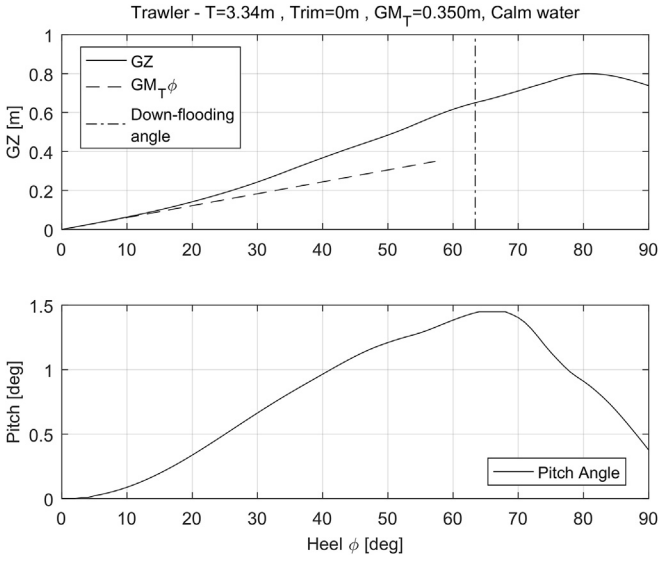

Fig. 2. Righting lever curve in calm water. Pitch is the Euler pitch angle, positive for bow down.

Table 2
Roll damping coefficients.

Linear roll damping coefficient (ν [−])	0.0187
Quadratic roll damping coefficient (β [1/rad])	0.393
Cubic roll damping coefficient ($\delta{\cdot}\omega_0$ [1/rad])	0.0

assumption, and taking into account the superstructures shown in Fig. 1. In addition, in Fig. 2, the Euler pitch angle corresponding to each heeling angle is also included.

In order to set up the nonlinear damping model, data from zero speed roll decay tests of a similar vessel have been used. Although, in principle, semi-empirical methods could be considered for this purpose (e.g. Ikeda's method (Himeno, 1981; Ikeda et al., 1978; Kawahara et al., 2009)), results from realistic data seem to be more reliable than those obtained from these approximations, at least for these type of vessels (Míguez González et al., 2015). The applied damping model is of the purely quadratic type, and coefficients are reported in Table 2. Such damping coefficients correspond to a configuration of the vessel without bilge keels, which is the configuration used in the present study.

These coefficients have been directly used in the 1-DOF models. However, in the 6-DOF model, due to the presence of couplings among different degrees of freedom and due to the presence of multiple submodels, a tuning process is necessary in order to fit the numerical roll decay to the target dissipation level. To this end, the drag coefficient $C_D(\mathbf{x})$ (see (12)) in the 6-DOF cross-flow model was assumed to have a uniform value of 0.8 on the centreplane. Afterwards, the linear ($B_{44L,add,O}$) and quadratic ($B_{44Q,add,O}$) roll damping coefficients of the additional roll damping moment (see (13)) were manually modified, whereas the cubic damping coefficient $B_{44C,add,O}$ was not used in the tuning. For each couple of tentative coefficients a roll decay was simulated and analysed to obtain the corresponding coefficients μ, β and δ. Such coefficients were then used, together with the natural roll frequency ω_0, to analytically calculate $\nu_e(A_{roll})$ according to (5) and to compare it with the target value obtained from (5) using the damping coefficients in Table 2. Fig. 3 shows a roll

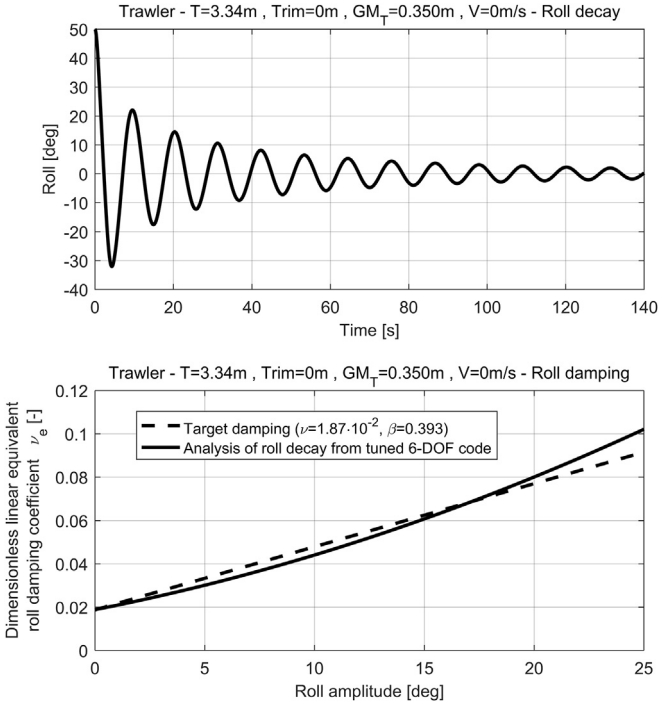

Fig. 3. Simulated roll decay from the 6-DOF model (top) and comparison of corresponding amplitude dependent dimensionless linear equivalent roll damping coefficient with target damping (bottom).

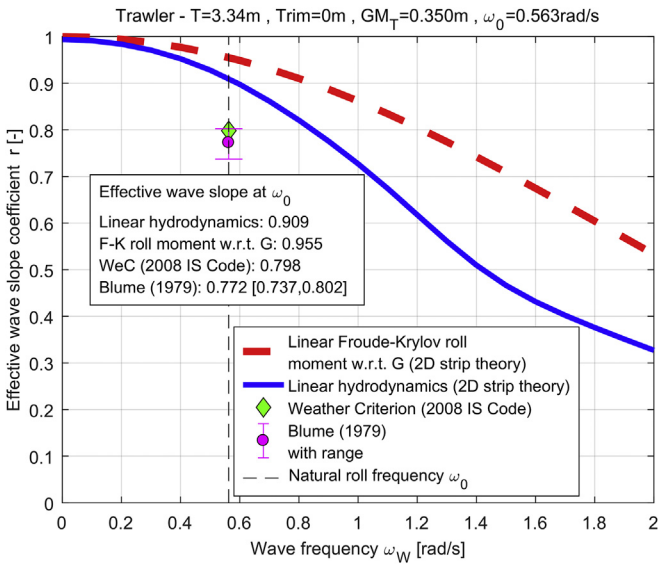

Fig. 4. Effective wave slope coefficient.

decay, and the corresponding dimensionless linear equivalent roll damping coefficient $\nu_e(A_{roll})$ compared to the target one, after the tuning process. As it can be appreciated, the results from the tuned numerical roll decay well match the target values.

Regarding the computation of the effective wave slope coefficient to be used in the beam seas 1-DOF model, four different alternatives have been applied, as it has been previously mentioned. These include a computation based on linear hydrodynamics (Bulian and Francescutto, 2009, 2011) accounting for yaw coupling), a calculation based on Froude-Krylov roll moment with respect to the centre of gravity, and the simplified semi-empirical methods proposed by Blume (1979) and by the IMO Weather Criterion (IMO, 2008a). In Fig. 4, the results obtained from these four methodologies are presented. The first two approaches, naturally account for the frequency dependence of the effective wave slope, which is therefore reported for the range $\omega_W = 0\,rad/s$ to $\omega_W = 2\,rad/s$. For the cases of the Blume and the IMO approaches, the effective wave slope coefficient is computed only for the natural roll frequency of the vessel ($\omega_0 = 0.563\,rad/s$). However, while the IMO Weather Criterion method provides a single value, the Blume method also provides a range around the estimated value. It can be noticed that, while the effective wave slope coefficient as predicted by the Blume method and by using the formulation from the IMO Weather Criterion are close each other, the two predictions are sensibly smaller than what can be obtained from the application of a linear hydrodynamic computation. Finally, it is worth underlining that, for the considered range of frequencies, the Froude-Krylov approach provides a conservative estimation of the effective wave slope coefficient compared to the other tested approaches.

3.2. Beam sea

This section presents and compares roll motion results, in regular beam seas, as obtained from the considered models.

Three values of wave steepness have been studied for a range of wave frequencies that includes the worst expected situations, which will occur in the vicinity of the 1:1 ratio of wave to natural roll frequency. In Table 3, the tested conditions are presented.

In Fig. 5, the results of the expected maximum roll amplitude values, obtained by applying the simplified analytical approach according to (4), and using the four different alternatives for the estimation of the effective wave slope coefficient, are shown.

Observing the results in Fig. 5, an estimation of the importance of the

Table 3
Reference test conditions. Regular beam waves.

Wave steepness (s_W)	[−]	1/100	1/50	1/30
Wave frequency (ω_W)	[rad/s]	0.113–1.126		
Frequency ratio $\left(\omega_W/\omega_0\right)$	[−]	0.2–2.0		
Wavelength to beam ratio $\left(\lambda_W/B\right)$	[−]	6.08-608		

methodology chosen for the computation of the effective wave slope coefficient can be made. As it can be appreciated, the difference in the maximum roll amplitude predicted by the different approximations is quite small, in absolute terms, for the lowest wave steepness. The divergence between the different alternatives starts becoming more noticeable for values of wave steepness over $s_W = 1/50$. However, the difference is within only ±1.6deg at a steepness $s_W = 1/30$, and within only ±1.9deg even at a steepness $s_W = 1/20$.

It can be also appreciated that roll amplitudes predicted by using the effective wave slope from the Blume and IMO Weather Criterion alternatives are almost coincident; the same happens among the linear hydrodynamics and the Froude-Krylov approaches. This is in line with results reported in Fig. 4, since damping is the same in all cases. Fig. 5 could therefore be considered to represent a sensitivity analysis of the expected outcome, in terms of predicted roll amplitude by the simplified method, taking into account the variability of effective wave slope coefficient depending on its prediction method.

In Fig. 6, the results of roll motion response are presented. The maximum roll amplitude, as a function of the frequency ratio, obtained for the three different wave steepness with the 1-DOF model (both absolute and relative angle alternatives) and the 6-DOF model, are reported. While in the 1-DOF models drifting effects are naturally not taken into account, in the 6-DOF simulations the vessel was restrained, as it is common to do, by soft springs and, to avoid dynamic interference, natural frequencies induced by the soft springs were checked to be well below the tested frequencies.

From the analysis of these response curves, some comments can be made.

If the response curves corresponding to the minimum analysed wave steepness (left figure, $s_W = 1/100$) are observed, it can be appreciated that the predicted amplitudes from the three alternatives are very close each other, although those obtained with the 6-DOF model are slightly larger than the others. In terms of frequency ratio, the three models

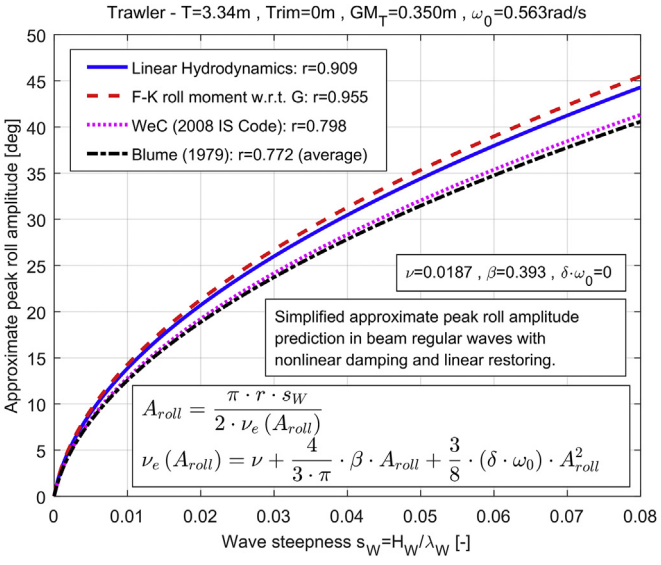

Fig. 5. Maximum roll amplitude as a function of wave steepness from the simplified approach. Beam regular waves.

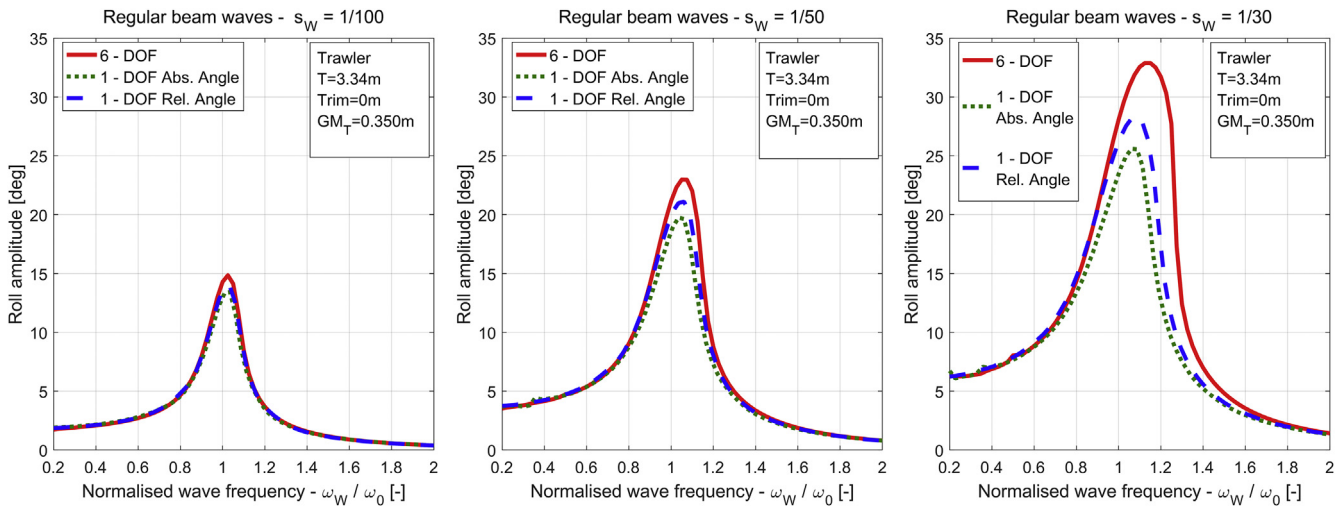

Fig. 6. Roll response in beam regular waves.

reproduce the larger motions at the same frequency value, slightly above $\omega_W/\omega_0 = 1.0$, with no appreciable response curve bending.

As the wave steepness is increased ($s_W = 1/50$), roll motion consequently increases, and the differences between the three models also become more noticeable. As it can be seen in the central plot in Fig. 6, the results from the 6-DOF model present a slightly higher and broader peak than those from the 1-DOF model. From the two 1-DOF alternatives, the absolute angle approach predicts the lowest amplitude, while the relative angle approach is between the other two models. Regarding the shape of the response curve, a bending to higher frequencies can be clearly observed in this test case, which was not significant in the previous one. However, differences among the three different models, both in amplitude and position of the peak, are in the range of 10% and can be considered as relatively small in absolute terms.

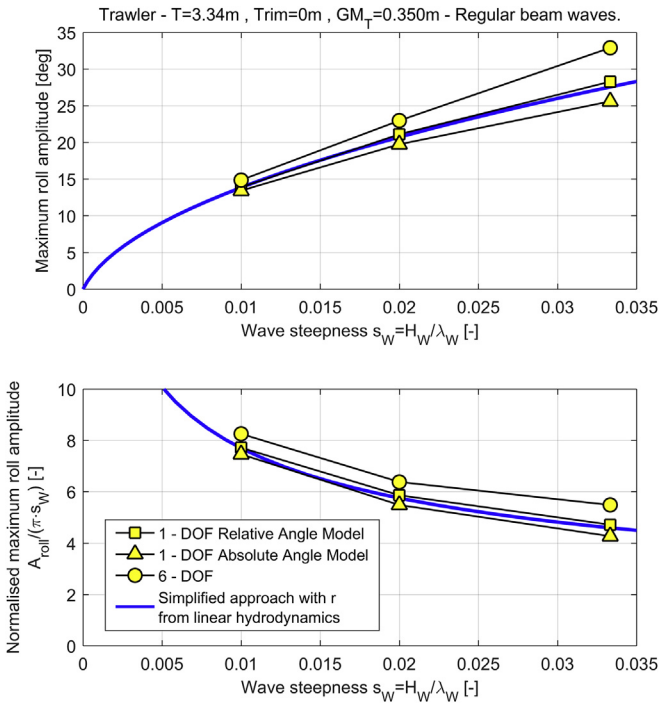

Fig. 7. Maximum roll amplitude (top) and maximum roll amplitude normalised by the wave slope (bottom), as functions of the wave steepness in beam regular waves.

Finally, in the right plot in Fig. 6, the results for the largest wave steepness ($s_W = 1/30$) are presented. As it can be appreciated, the differences between the three models become much more noticeable now, especially between the 6-DOF model and the other two, not only in the peak amplitude, but also in its position and width. The bending of the response curve is also larger in the case of the 6-DOF. The differences between the two alternatives of the 1-DOF model, although slightly larger than in the previous tests cases, are still not very significant.

Overall, it is worth underlining that, among the 1-DOF models, the relative angle one shows a tendency closer to the behaviour shown by the 6-DOF model.

In Fig. 7, the maximum roll amplitudes, as obtained from the response curves computed with each model as a function of wave steepness, are shown. In order to better highlight nonlinear effects, the same figure also shows the maximum roll amplitude in radians normalised by the wave slope $\pi \cdot s_W$. This summary plot is useful in those cases where the maximum roll amplitude of the vessel is of interest, for varying wave steepness and regardless of the frequency ratio at which it occurs (like in the Weather Criterion). In addition to the results from the time domain mathematical models, results obtained from the analytical approach (4) using the effective wave slope coefficient calculated through linear hydrodynamics are also presented.

As it can be appreciated, for the lowest steepness under consideration, the predictions obtained by the three studied alternatives are very close each other. Moreover, also the simplified analytical approximation provides very close results. However, as the wave steepness increases, the difference between the three alternatives increases as well, in accordance, of course, with results in Fig. 6. Among the 1-DOF models, the one better matching 6-DOF results is the relative angle one. Since the two 1-DOF models share the same damping term, the observed difference among them can therefore be directly linked with the differences in the restoring/forcing terms. In fact, the 1-DOF absolute angle model applies the nonlinear *GZ* function in the restoring term only to the absolute roll angle ϕ, keeping the wave forcing as an external sinusoidal forcing $\omega_0^2 \cdot \alpha_{eff}(t)$ (see (1)). On the other hand, in the relative angle model, the nonlinear *GZ* function is applied to the difference $\phi - \alpha_{eff}(t)$ (see (3)). If, for the sake of explanation, it is imagined that *GZ* is described by a polynomial representation, it can be immediately understood that the relative angle model implicitly introduces additional terms in the equation of motion compared to the absolute angle model. These additional terms, eventually, influence the dynamics of the system and are the source of the observed differences (Belenky and Sevastianov (2007) and Bulian and Francescutto (2011) presented, in the past, discussions following this line of reasoning). From a general perspective, results in

Table 4
Reference test conditions. Regular head waves.

Wave Steepness (S_W)	1/200	1/100	1/50	1/30	1/20	1/15
Wave Frequency (ω_W)	0.845–1.689 rad/s					
Frequency Ratio $\left(\omega_W/\omega_0\right)$	1.5–3.0					
Wavelength to Ship Length Ratio $\left(\lambda_W/L_{PP}\right)$	2.980 – 0.745					

Figs. 6 and 7 highlight that the 6-DOF model tends to show systematically larger peak rolling amplitudes compared to the 1-DOF models at all tested steepnesses, with differences which increase as the wave steepness increases. Considering that the peak amplitude of the roll response is, loosely speaking, the result of the combination of a forcing action and a dissipation action, the systematic effect observed from the simulations could be due to the fact that the overall level of dissipation in the 6-DOF model during simulations in waves is smaller than the level of dissipation of the 1-DOF models, due to the fact that the overall forcing due to waves in the 6-DOF simulation model is larger than the forcing in the 1-DOF models, or a combination of these two effects. In addition, looking at the fact that also the two 1-DOF models, which are characterised by the same damping term, show different outcomes, it could also be conjectured that part of the observed differences between the 6-DOF model and the 1-DOF model could come from the effect of nonlinear Froude-Krylov forces. Looking at Fig. 7, it is also interesting to comment that the results from the 1-DOF relative angle model are practically coincident with those obtained from the simplified analytical approach for the whole range of studied wave steepnesses. This fact is very relevant if some of the proposed approaches are intended to be used during the early design stage of the considered type of vessels. In fact, whenever only an indication of the largest expected roll motion in regular beam waves is needed for a given design, then the use of a simplified analytical approach, such as the one used in this case, could be almost equivalent to the use of a more complex alternative, such as the 1-DOF relative angle model. On the other hand, if the whole frequency response is of interest for a given design, a more complex approach shall be used, and the observed dispersion of results for the largest tested steepness indicate that caution should be exercised when predicting roll amplitudes for too severe approaches, since prediction uncertainty could be non-negligible.

3.3. Longitudinal sea

In this section, the results of roll motion obtained by using the considered different models in regular head waves are reported.

Six different wave steepness values have been tested, with frequency ratios ranging from $\omega_W/\omega_0 = 1.5$ to $\omega_W/\omega_0 = 3.0$, and corresponding wave to ship length ratio λ/L_{pp} between 0.745 and 2.980. Table 4 presents an overview of the tested conditions.

As it is well known, the phenomenon of parametric roll resonance is generated by the effect that wave passing has on the underwater hull geometry of the vessel and, subsequently, on her righting lever curves and initial stability. The typical conditions in which parametric roll resonance is more severe is in wave frequency to natural roll frequency ratios of around $\omega_W/\omega_0 = 2.0$, and in wavelengths similar to the ship length ($\lambda_W \approx L_{PP}$). These conditions are those in which wave passing is typically more effective in promoting the inception of parametric roll, as a consequence of the combination of the frequency condition with a sufficiently large magnitude of the restoring variations. The magnitude of the parametric roll phenomenon is directly related to the amplitude of the variation of the vessel roll restoring parameters, also known as parametric excitation, when these occur with the appropriate frequency.

Fig. 8 shows the variation of the vessel metacentric height (GM_T), as a function of the longitudinal coordinate of the wave crest along the hull (x_c), for different wave steepness and a wave length $\lambda_W = L_{PP}$. In this figure, x_{app} represents the longitudinal coordinate of the aft perpendicular of the vessel and L_{pp} is the ship length between perpendiculars.

Fig. 9 provides the same information for a wave corresponding to a frequency ratio of $\omega_W/\omega_0 = 2.0$. The presented data have been obtained applying the two methodologies which have been implemented for the determination of the righting lever in the 1-DOF model: free trim and fixed trim calculations.

In case of a wavelength equal to the vessel length (Fig. 8), the maximum metacentric height values coincide with wave crest placed in the vessel perpendiculars (i.e. through amidships), while minima occur while wave crest is near amidships. In addition, the expected relationship between the amplitude of GM_T variation and wave steepness can be observed, with an increase of the parametric excitation as the wave steepness increases. If the results obtained by using the free trim and the fixed trim approach for the calculation of the vessel righting lever in waves are compared, it can be appreciated that, in terms of amplitude, both results are quite similar for the lower steepnesses, and variations obtained from the fixed trim approach are slightly larger for the largest steepnesses. If the position of the peaks is analysed, a light bending and displacement to the right can be noticed in the fixed trim case, which is not present in the free trim calculations. In any case, both alternatives provide very similar outcomes.

However, the similarities among the two calculation approaches reduce if the wavelength under study is increased (Fig. 9). In this case, the results obtained for the wavelength $\lambda_W = 48.615\ m$, corresponding to a frequency ratio of $\omega_W/\omega_0 = 2.0$ in free and fixed trim conditions, are noticeably different. On the one hand, fixed trim variations of metacentric height are larger than free trim ones, for all wave steepnesses. On

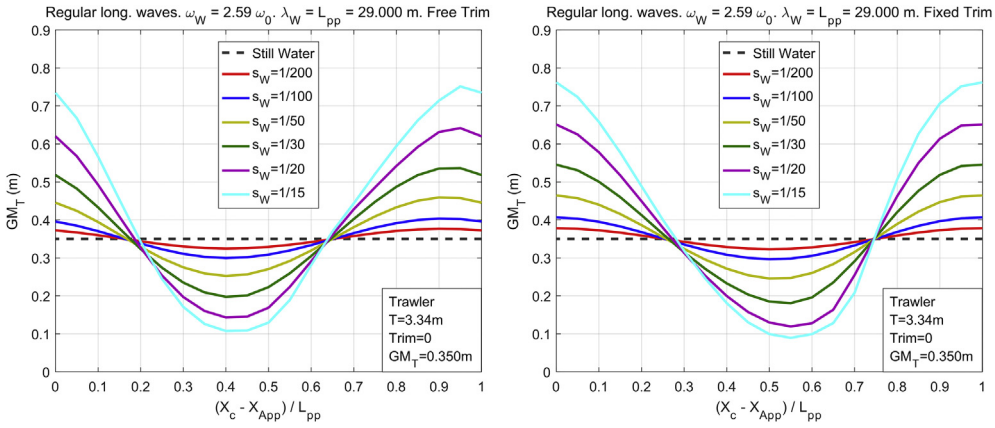

Fig. 8. GM_T variation in regular longitudinal waves as function of wave crest position. $\lambda_W = L_{PP}$ corresponding to $\omega_W = 2.59{\cdot}\omega_0$. Left: free trim. Right: fixed trim.

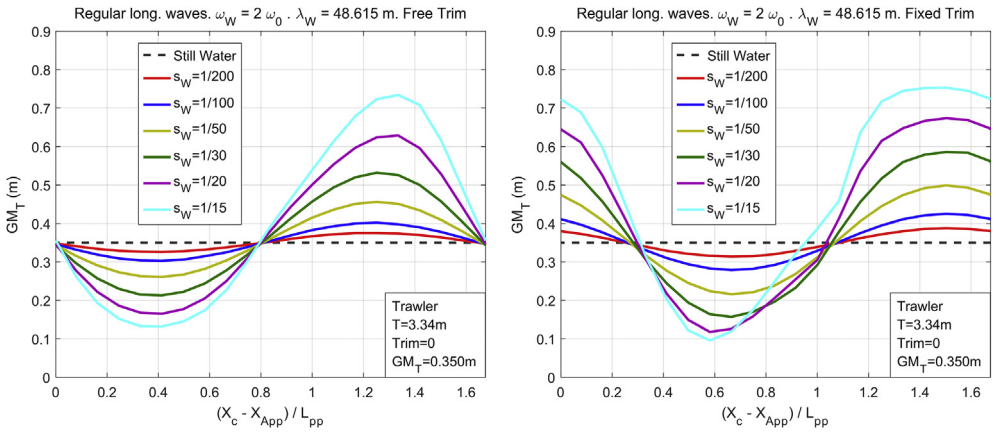

Fig. 9. GM_T variation in regular longitudinal waves as function of wave crest position. $\lambda_W = 48.615\ m$ corresponding to $\omega_W = 2{\cdot}\omega_0$. Left: free trim. Right: fixed trim.

the other hand, regarding the peak positions, a large shift to the right can be observed in the fixed trim case. Finally, and especially for the largest steepnesses, fixed trim curves of GM_T as a function of the wave crest position, present wider peaks than those obtained from the free trim calculations.

In addition to the GM_T variation due to wave passing for a fixed wave length and different wave crest positions and steepnesses, as shown in Figs. 8 and 9, in Fig. 10 the variation of GM_T due to the effect of waves as a function of wavelength and frequency ratio, for the different values of wave steepness, and for the free to trim and fixed trim methodologies, is presented. Moreover, in Fig. 11 the mean GM_T in waves as a function of wavelength and frequency ratio, for the different wave steepnesses and for the free to trim and fixed trim methodologies, is included.

As it can be appreciated from these figures, the variation of GM_T in waves tend to be larger in the fixed trim case, and this difference becomes more noticeable as wavelength is increased. Regarding mean GM_T in waves, a similar behaviour could be observed, and the difference between the fixed trim approach and the free trim one becomes very large as wave length and wave steepness increase.

The patterns shown in Figs. 8 and 9 for the metacentric height are reflected by the righting lever curves in waves. As an example, the GZ curves (both free and fixed trim) for the wave condition with largest steepness and wavelength equal to ship length ($\lambda_W = L_{PP}$, $s_W = 1/15$), are shown in Fig. 12 as colour plots as a function of wave crest position and roll angle. As it can be appreciated, in the case of free trim, the maximum GZ values are associated to a wave crest position close to the vessel perpendiculars (wave through amidships), while minimum values are placed when it is around a 40% of the wavelength from the aft perpendicular. These wave crest positions basically coincide with those observed for minimum and maximum metacentric height in Fig. 8. In the

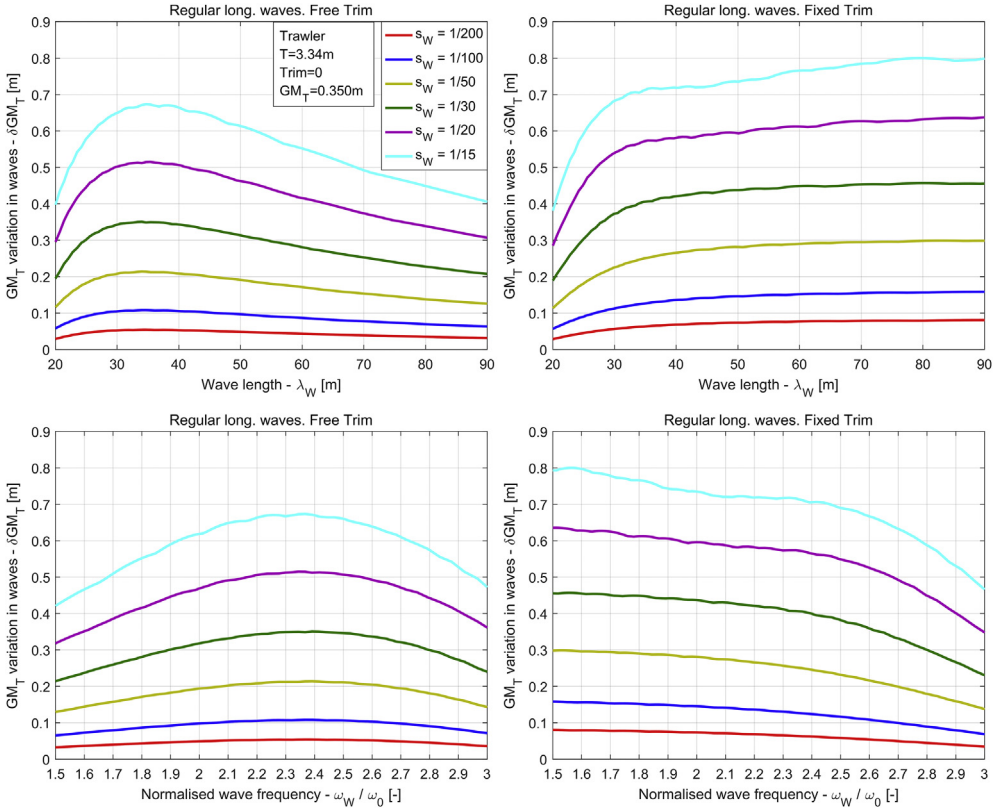

Fig. 10. GM_T variation in regular longitudinal waves as function of wave length (top) and of normalised wave frequency (bottom), for different wave steepnesses. Left: free trim. Right: fixed trim.

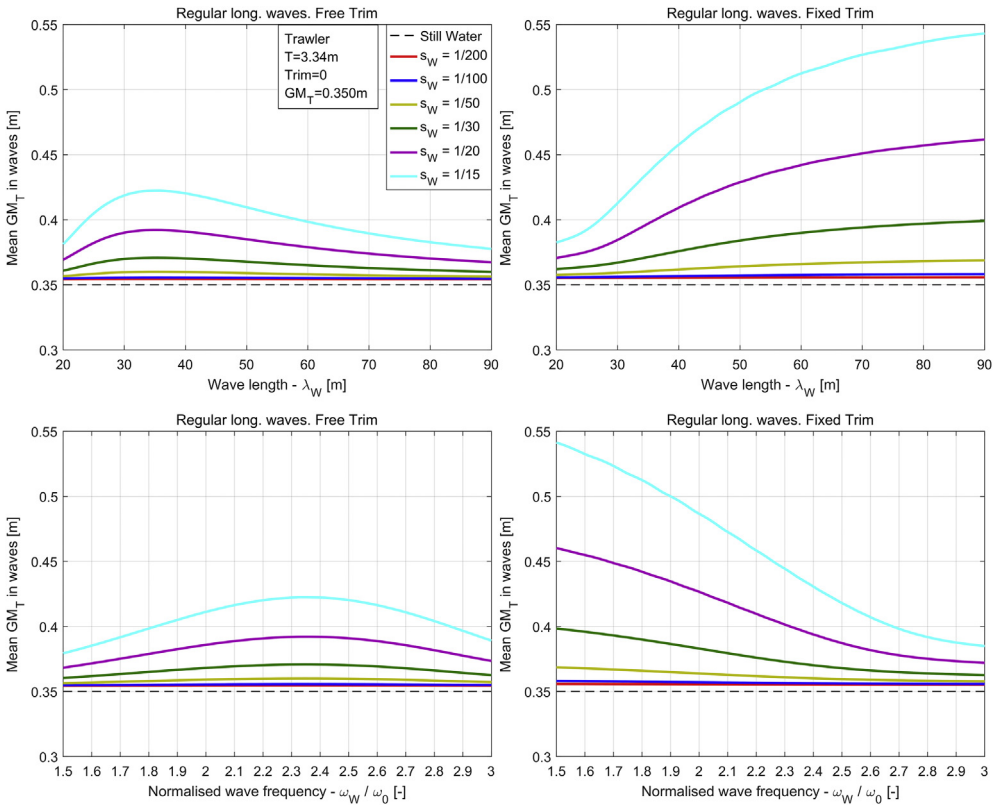

Fig. 11. Mean GM_T in regular longitudinal waves as function of wave length (top) and of normalised wave frequency (bottom), for different wave steepnesses. Left: free trim. Right: fixed trim.

case of fixed trim, larger values of maximum GZ are observed in comparison to the free trim case. Although the positions of these maxima are similar to those on the free trim case, the minimum values are shifted up to a position at around 60% of the ship length from the aft perpendicular. This pattern could also be observed in Fig. 8, where the presence of a bending to the right of the GM_T curves, as a function of the wave crest position, was already highlighted. In addition to this, a shifting of the minimum values to wave crest positions closer to the aft perpendicular at large roll angles can be observed. This behaviour is not present in the free trim calculations, where minima occur approximately at the same position almost independently of roll angle.

In addition to GM_T and GZ data in waves which have been described, Fig. 13 shows the normalised variation of KM_T due to wave passing for different values of wavelength and steepness, in the free trim case. These curves provide information regarding the amplitude of the variation of the transverse stability characteristics of the vessel for given wave condition, normalised by using the wave amplitude. These values can be considered to represent a sort of approximate numerical transfer function between wave excitation and parametric excitation, while a semi-analytical approach for their calculation was presented in the past by Dunwoody (1989). As it can be observed, the influence of wave steepness on the magnitude of normalised KM_T variation is noticeable only in the vicinity of a wavelength similar to vessel length, that is where maximum values occur. It is noted that additional relative maxima also take place at wavelengths close to 12 m (around 40% of the ship length between perpendiculars), although their amplitude is noticeably lower than that of the absolute ones.

It is however to point out that, for the vessel used in this study, the observed almost linear dependence of the variation of KM_T from the wave steepness, for the considered waves, could be associated with the fact that the considered vessel has a large freeboard. However, in case of fishing vessels characterised by small freeboard, and depending on the considered wave amplitudes, the linear modelling could fail to properly represent the variation of KM_T in waves. In such cases a more general nonlinear dependence, based on direct calculations, should be accounted for.

Fig. 13 also reports the largest value of normalised KM_T variation for a wave frequency of $\omega_W = 2{\cdot}\omega_0$ ($\lambda_W = 48.615\,m$), which corresponds to the lowest wave steepness ($s_W = 1/200$). This value has been conservatively taken to correspond to the f_1 factor in the simplified methodology (see (8)) for predicting roll motion amplitude under parametric roll conditions in head seas. Results from the application of the simplified methodology are shown in Fig. 14. The figure shows the predicted rolling amplitude as a function of wave steepness for a wave frequency $\omega_W = 2{\cdot}\omega_0$. As it can be observed, roll motion under parametric roll starts developing above the inception threshold which, in this case, corresponds to a wave steepness slightly higher than $s_W = 1/200$. For larger steepnesses the roll motion amplitude grows up linearly with the steepness up to more than 50 degrees at $s_W = 1/20$. The linear increase of roll, as predicted by the simplified methodology, is a direct consequence of the assumption of linear-plus-quadratic roll damping model. If a cubic roll damping term was added, the predicted roll amplitude would show a reduced grow rate for larger steepnesses. It is also important to recall that the simplified methodology (8) neglects the effect of nonlinearities in the restoring term. Since nonlinearities of the restoring typically lead to a shifting of the peak of the parametrically excited roll response curve as the excitation, and thus the amplitude of roll, increases, this effect is not captured by the simplified methodology (8).

Comparisons of predicted roll motion in regular head seas obtained by using the 6-DOF and the 1-DOF models (free and fixed trim GZ calculation), are presented in Fig. 15, where the roll amplitude is plotted against ω_W/ω_0 ratio for the six tested wave steepness. Similarly to the case of beam waves, also in this case, the 1-DOF naturally enforce the zero speed, mean zero-yaw condition. In order to achieve a similar situation also in case of 6-DOF simulations, soft restraints were added. In particular, the ship is restrained by two elastic lines connected, on one

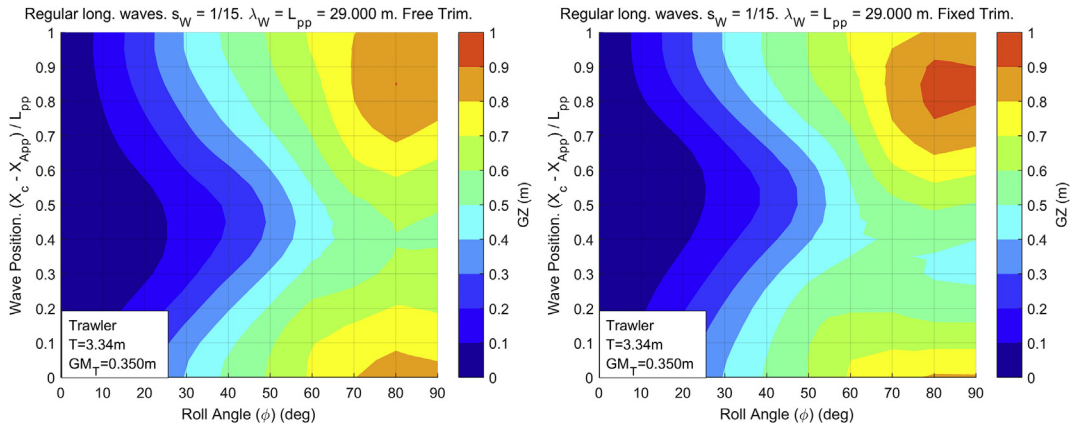

Fig. 12. GZ variation in regular longitudinal waves as function of wave crest position and roll angle. $\lambda_W = L_{PP}$ ($\omega_W = 2.59{\cdot}\omega_0$), $s_W = 1/15$. Left: free trim. Right: fixed trim.

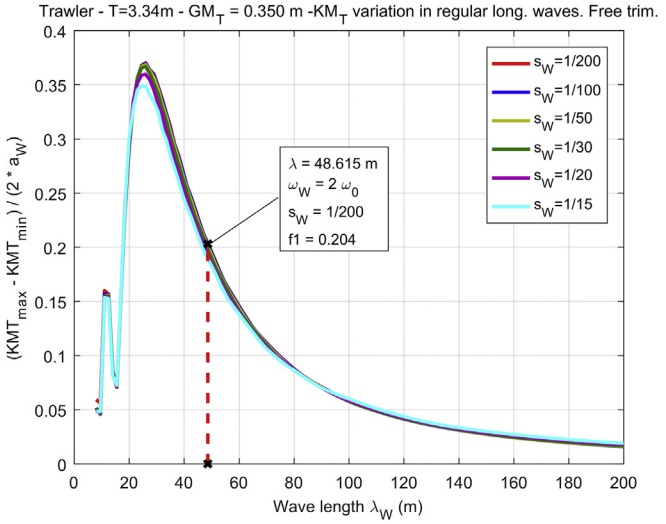

Fig. 13. Normalised variation of KM_T as a function of wave length and wave steepness. Free trim calculations.

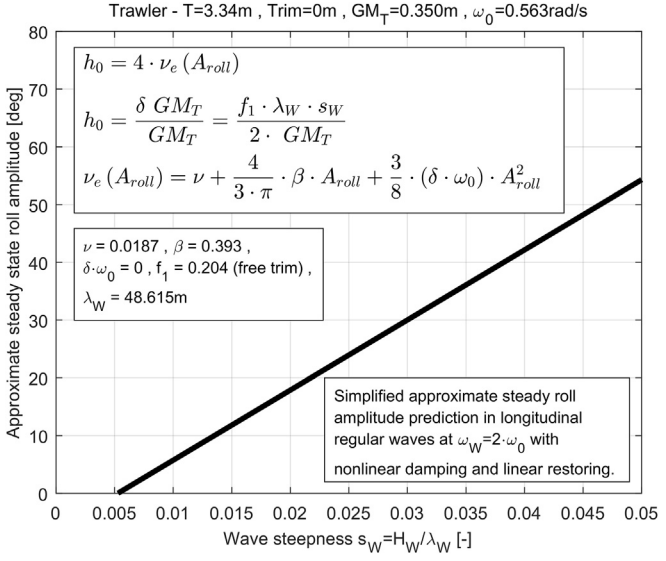

Fig. 14. Maximum roll amplitude as a function of wave steepness from the simplified approach. Head regular waves.

end, at the ship bow at the calm water draught, and fixed to the earth-fixed reference frame on the other end, in a v-shaped configuration. The elastic lines produce force when in traction, but do not produce force in case of compression, similarly to elastic lines used in real experiments. Similar elastic lines where not connected at the stern, since, due to the zero-speed and head sea condition, this was found not necessary, and it was therefore preferred to reduce at minimum the number, and thus the influence, of the restrain system.

As it can be appreciated from Fig. 15, in the $s_W = 1/200$ case, the only model which shows appreciable roll motion is the 1-DOF fixed trim one, mainly due to the fact that the parametric excitation in this case, as was shown in Figs. 9 and 10, is larger (almost doubled) than that of the 1-DOF free trim model. It can also be noted that the peak amplitude occurs at $\omega_W/\omega_0 = 2$, due to the fact that, for small rolling amplitude, *GZ* is well approximated by its linear approximation, and hence no roll response bending occurs.

As the wave steepness is increased, the roll amplitudes predicted by the three models increase as well. Up to a wave steepness of $s_W = 1/50$, the response curves obtained from the 1-DOF model with free trim and the 6-DOF model are almost coincident. On the other hand, the amplitudes predicted by the 1-DOF fixed trim model are systematically larger and the unstable area in this case is also wider than for the 6-DOF and 1-DOF free trim models. These are consequences of the larger parametric excitation in the fixed trim 1-DOF model, as can be observed also in Fig. 10. As the predicted roll amplitudes increase, the effect of the *GZ* nonlinearities can be appreciated in the bending to the right (higher wave frequencies) of the response curves. This is a characteristic which is obtained with all the models, which is in line with the hardening calm water restoring, and which increases with the roll amplitude (as *GZ* nonlinearities become more relevant).

If the wave steepness is further increased ($s_W = 1/30$), a different behaviour is observed for each of the models. In the low frequency/long waves range (left part of the plot), the inception of parametric roll starts nearly at the same frequency ratio for the three models and the predicted roll amplitudes remain very similar up to a frequency ratio of approximately $\omega_W/\omega_0 = 2.0$. For larger frequencies the predicted roll amplitudes start diverging, being the highest those predicted by the 1-DOF fixed trim model, and the smallest those from the 6-DOF model.

Finally, a third different behaviour is observed for the highest wave steepnesses ($s_W = 1/20$ and $s_W = 1/15$). In these cases, although the inception frequency ratios of parametric roll are quite similar in the 6-DOF model and 1-DOF model with free trim, the parametric roll inception range is sensibly shifted to higher frequencies in the 1-DOF fixed trim case, and this is particularly noticeable for the highest tested wave steepness. Up to a frequency ratio around $\omega_W/\omega_0 = 2.0$, the response curves for the 6-DOF model and the 1-DOF free trim model remain quite close, similarly to what has been previously observed. However, also in this case, response curves start to diverge for higher frequencies. While

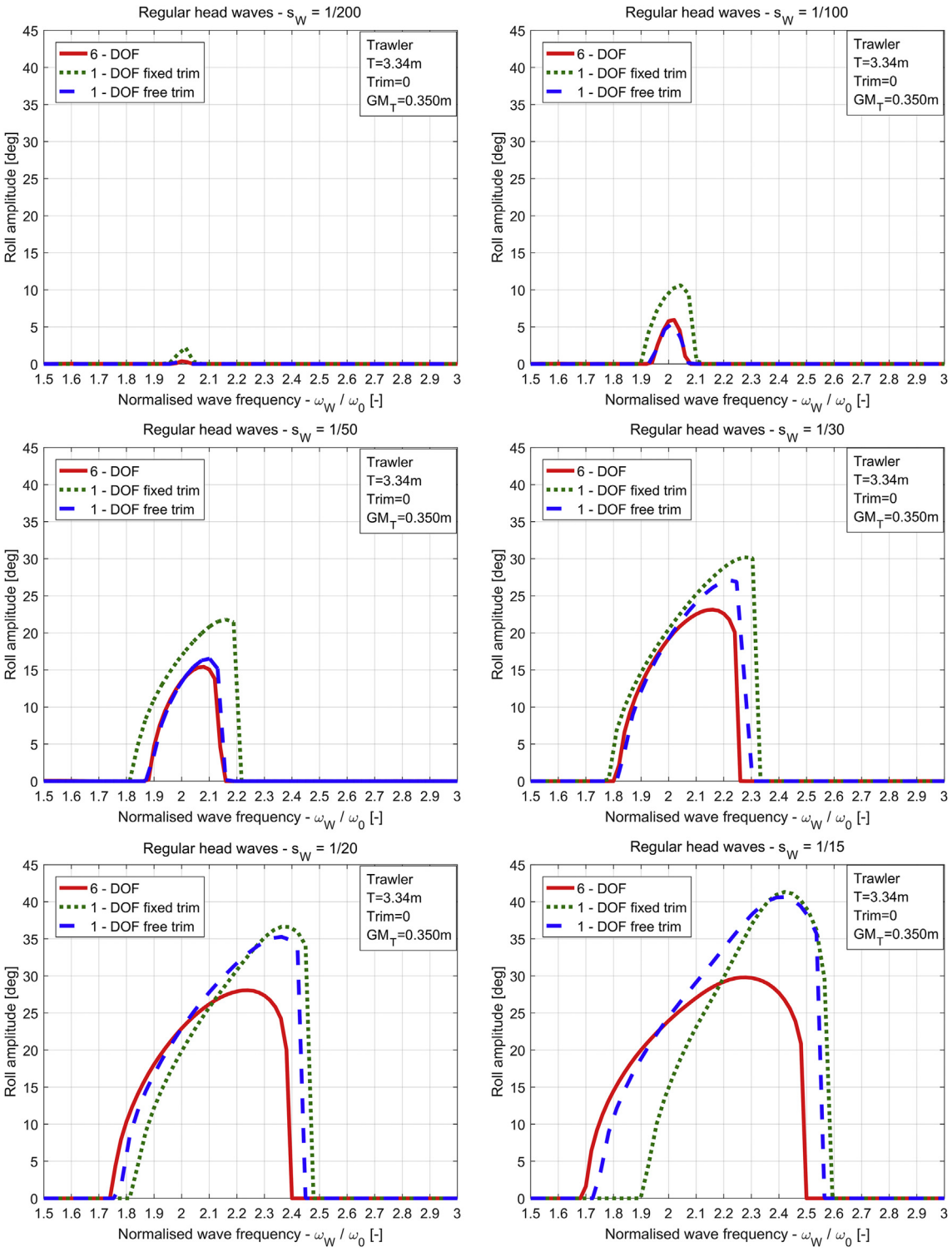

Fig. 15. Roll response in head regular waves.

the 6-DOF model tends to saturate and the maximum roll amplitude does not increase much as the wave steepness is increased, the roll amplitude predicted by the 1-DOF free trim model continues increasing with wave steepness. At the same time, the maximum roll predicted by the 1-DOF fixed trim model tends to show a stronger saturation effect compared to the free trim one. Eventually, the response curves of both alternatives of the 1-DOF model reach similar maxima and have approximately the same shape in the region of frequencies from around $\omega_W/\omega_0 = 2.3$ and above. Regarding the instability areas, they are similar in width when comparing the 6-DOF and the 1-DOF free trim models, although that of the latter is slightly shifted to higher frequencies. However, the instability area obtained using the 1-DOF fixed trim model is noticeably narrower at the largest wave steepness.

Such behaviour, however, is associated with the indirect effect of the variation of mean GM_T in waves. The variation of mean GM_T in waves ($GM_{T,mean,W}$), if compared to the nominal one in calm water, can be considered to basically correspond to a change of the reference natural frequency of the vessel, which is relevant for the determination of the

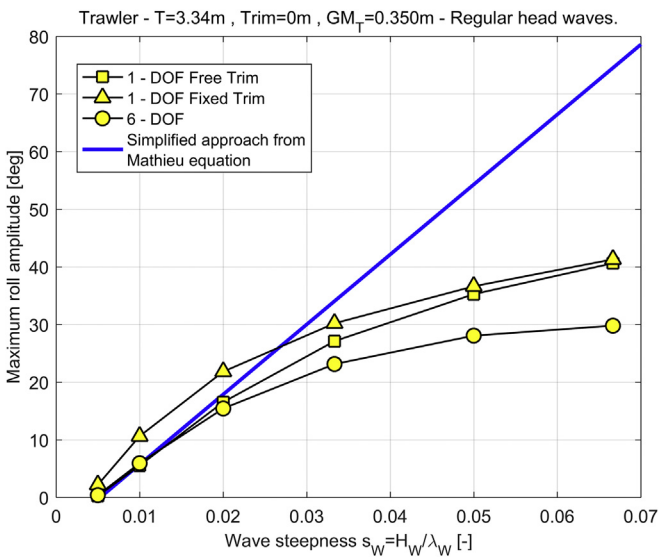

Fig. 16. Maximum roll amplitude as a function of wave steepness in head regular waves.

tuning ratio. This reference natural frequency, when wave effects are taken into consideration ($\omega_{0,W}$), becomes:

$$\omega_{0,W} = \omega_0 \cdot \sqrt{\frac{GM_{T,mean,W}}{GM_T}} \tag{14}$$

As a result, the nominal tuning ratio ω_W/ω_0, which is normally used for plotting the results, is no longer a good approximation of the actual tuning ratio in waves, $\omega_W/\omega_{0,W}$.

It is also to be noted that the actual amplitude of parametric excitation is $\frac{\delta GM_T}{GM_{T,mean,W}}$, and this quantity depends on both the wave length and the wave steepness, which is further affecting the observed behaviour.

Finally, again, the effect of *GZ* nonlinearity can be observed in the bending to higher frequencies of the roll amplitude curves from the three models.

In Fig. 16, the maximum roll amplitudes obtained with the three models for the six tested wave steepnesses, are compared. This figure is useful for analysing the maximum expected roll amplitudes in head waves, without focussing on the wave frequency at which this maximum occurs. For sake of comparison, the results obtained with the simplified analytical approach, based on the Mathieu equation with nonlinear damping, have also been included.

Observing the results reported in Fig. 16, it can be seen that the values obtained with the fixed trim 1-DOF model are the highest from the three approaches in the whole range of wave steepness, as it has been already mentioned. Regarding the other two models, the results obtained with the free trim 1-DOF model are very similar to those obtained with the 6-DOF in the lowest range of wave steepnesses. However, the difference between these two models becomes larger as wave steepness increases, and for the highest values of wave steepness the results from the free trim 1-DOF model are in line with those of the fixed trim approach. The simplified approximation accurately tracks the results of the more complex models in the low range of wave steepnesses, especially those of the 1-DOF free trim one, as the applied f_1 transfer function has been determined in line with this model for low steepnesses. Due to the increased level of parametric excitation, the 1-DOF fixed trim model shows, instead, an earlier build-up of roll. However, as wave steepness increases, the simplified methodology, which neglects the nonlinearities of roll restoring, predicts much larger amplitudes than those obtained by any of the proposed models. This confirms the importance of restoring nonlinearities in determining the amplitude of parametrically excited roll motion in regular waves. It is interesting to note that, contrary to what was observed in the beam sea case (compare with Fig. 7), here in the head sea case the 6-DOF model tends to show the smallest maximum roll amplitudes, with the exception of the two smallest tested wave steepnesses where, however, the 6-DOF model shows results which are only marginally larger than the 1-DOF free trim model. Although it was not possible to identify a clear source for the observed behaviour of the 6-DOF model with respect to the 1-DOF ones, some aspects could be linked with the observed outcomes. One point is that the 6-DOF model takes into account the actual dynamics of heave and pitch, whereas the 1-DOF free trim model considers them quasi-statically, and the 1-DOF fixed trim model considers only heave quasi-statically and fixes the trim. Another source of differences could be the fact that the 6-DOF model provides an explicit dynamic coupling between all relevant degrees of freedom. Instead, in the 1-DOF models, this dynamic coupling effect is neglected or it is approximately accounted for in an implicit way (coupling between sway, roll, and yaw). It is also possible that, as a result of the differences in modelling and as a result of coupling, the 6-DOF approach in the simulations in waves is associated with a dissipation level which eventually differs from that of the 1-DOF models.

4. Discussion and final remarks

The limitations in cost, time and a simplified regulatory framework, usually limit the application of too complex tools within the design process of fishing vessels. However, the inception of parametric roll in longitudinal waves or excessive roll motions in beam seas, are well-known phenomena which could affect the operational safety of this type of vessels. The application of simple models could therefore help in addressing the risk stemming from these phenomena, within the mentioned practical constraints.

The main objective of this paper was, therefore, to compare the performance of simplified 1-DOF models, as well as very simplified analytical formulations, with respect to outcomes from more complex 6-DOF high fidelity blended modelling, for analysing the vulnerability of the vessel to parametric roll resonance and large motions in beam seas. Such comparison was carried out to analyse the suitability of the former methods to be used during the early design stages, where the application of any stability analysis tool should fulfil some requirements of reduced cost, time and complexity, and 6-DOF codes are therefore out of the scope. This is particularly true in the case of fishing vessels, which are the specific target of the present study.

To this end, the roll motion response of a mid-sized trawler, at zero speed and for regular beam and head waves with different steepness and frequencies, was analysed by applying a state-of-the-art 6-DOF model and different simplified nonlinear 1-DOF models. For the 1-DOF modelling, two methodologies were applied in the beam waves case (absolute and relative angle modelling for the excitation and restoring terms), and another two in the longitudinal waves case (based on fixed trim and free trim calculation of righting lever in waves). In addition to this, two very simplified analytical expressions to compute the maximum expected roll amplitude, both in longitudinal and beam regular waves, have been also applied.

4.1. Beam waves condition – harmonic resonance

The obtained results show that, for the case of beam seas, even the simplest fully analytical approach which was applied, based on linear restoring and nonlinear damping, could be considered as well reproducing the outcomes from the most complex alternative if only an estimation of the maximum roll amplitude is needed. The estimation of the maximum roll amplitude could be very useful, for example, to reduce the risk of flooding through open doors or through progressive flooding points, which are known to be very likely causes of fishing vessel accidents (CIAIM, 2014; Wolfson Unit, 2004). In this case, the use of the simplified analytical approach could already help in applying possible corrective measures to the vessel design aimed at avoiding, or at least

reducing, these issues. This approach is also in line with the background theory of the existing Weather Criterion. If the whole response curve is of interest, then the 1-DOF model based on a relative angle approach provided the closest results to the 6-DOF model. The differences in the predictions were larger as the forcing wave steepness increased.

In addition to the above, it is worth making some comments regarding the estimation of the effective wave slope coefficient, which is needed in both of the simplified methodologies. The main approach applied in this work for the determination of such coefficient, which has been proved in the past to be effective and theoretically justifiable, is based on linear hydrodynamics. However, such methodology requires linear hydrodynamic data, which might not available in case of typical fishing vessels design, unless seakeeping calculations are carried out. Simplified alternatives have also been investigated, which are based on direct Froude-Krylov pressure integration or semi-empirical formulae. For the tested case, the Froude-Krylov approach could be a good balance between simplicity and accuracy. In fact, it allows providing a frequency dependent effective wave slope function, and, in the range of frequencies of interest for the study, it was conservative with respect to the approach based on linear hydrodynamics. On the other hand, semi-empirical methodologies provided effective wave slope coefficients only at the roll natural frequency, which were also non-conservative with respect to the other tested methodologies.

4.2. Longitudinal waves condition – parametric roll

Regarding parametric roll resonance, the situation is different with respect to that discussed above for the beam sea case. The very simplified analytical approach used herein, based on linear time dependent roll restoring and accounting for nonlinearities only in damping, proved to be unsuitable for predicting the rolling amplitudes above parametric roll threshold, apart from regions of very small steepnesses. For moderate/large wave steepness, the use of at least a 1-DOF model was necessary for the tested case. If only the maximum roll amplitudes are needed, the use of the 1-DOF fixed trim model represented, for the tested case, a conservative and thus on-the-safe-side approach compared to the 6-DOF model. In fact, the former overpredicted roll motion in comparison to the latter in the whole range of wave steepnesses. If the details of the roll response curve are of interest, the 1-DOF free trim model showed closer results to the blended 6-DOF code, although the observed differences increased for larger wave steepnesses.

4.3. Practical implementation

From the point of view of implementation, some comments can be made. For the beam sea case, if the 1-DOF time domain methodology is considered, the implementation of the model requires the computation of the *GZ* curves in still water, the prediction of the effective wave slope coefficient and the vessel roll damping. The 1-DOF approach is, of course, much more affordable, in terms of required technical skills, time and cost, if compared to the use of blended 6-DOF tools. The implementation of the fully analytical simplified approach is even simpler, only needing the effective wave slope coefficient and the equivalent roll damping. Although the computation of effective wave slope coefficient through linear hydrodynamics is likely too complex considering the typical fishing vessel design routine, the use of the simplified Froude–Krylov approach is a much easier alternative once the hull geometry and the vessel loading condition are available, as it is always the case during design stages. Following these considerations, it can then be stated that the implementation of these models (1-DOF time domain model and fully analytical method) within typical existing tools, does not present any serious difficulty, and will be a very straightforward process.

For the longitudinal sea case, the evaluation of parametric roll on the basis of the 1-DOF model, requires the computation of several surfaces of *GZ* for different waves. Although these are relatively simple computations, they require a naval architecture software which is capable of performing them in a properly automated way. This is a level of complexity higher than the calculations of righting lever in calm water, as it is not usually built-in in standard software, and therefore makes the whole process of setting up the 1-DOF model for parametric roll more time consuming than that for the beam waves case. Although the implementation of the analytical approach is much simpler, its performance, as it has been already discussed, is far from satisfactory for most of the tested conditions.

4.4. Final remarks

Considering the envisioned practical application of the proposed alternatives, it could therefore be concluded that simple models can provide reasonable predictions, with much lower effort, compared to the use of the more complex 6-DOF tool in the initial stages of the vessel design. However, their real applicability, as typical, is largely dependent on their implementation in a self-contained software application, with a user friendly interface and high level of automation, simplifying, therefore, the process of model setting up and use. This is an aspect which is particularly important in the case of fishing vessels design.

For obtaining realistic roll predictions, accurate roll damping information is necessary, and this is valid, of course, for both the beam sea case, as well as for the longitudinal sea case. Use of damping coefficients from a similar vessel, application of analytical methods, or even the use of a real vessel roll decay test, could be different alternatives for obtaining these data. At the moment, however, there seems to be no widespread and accepted methodologies for this purpose, which are applicable to fishing vessels, and research is therefore needed in this respect.

Finally, it has to be indicated that this study is limited to one single vessel and therefore, its conclusions cannot be extended to the whole fishing fleet, where different typologies and sizes may be found. Nevertheless, in case the maritime authorities would undertake a major review of the fishing vessels stability regulatory framework to incorporate direct assessment approaches, the basis established in this work would be of direct application.

Acknowledgements

Part of the present work was carried out during a research visit at University of Trieste, supported by the Spanish Ministry of Education, Culture and Sport (http://www.mecd.gob.es) under the “José Castillejo” program, grant CAS16/00013.

References

ABS, 2004. Guide for the assessment of parametric roll resonance in the design of container carriers. Am. Bureau Shipp.

Ayaz, Z., Vassalos, D., Spyrou, K., 2006. Manoeuvring behaviour of ships in extreme astern seas. Ocean. Eng. 33, 2381–2434.

Bačkalov, I., Bulian, G., Cichowicz, J., Eliopoulou, E., Konovessis, D., Leguen, J.F., Rosén, A., Themelis, N., 2016. Ship stability, dynamics and safety: status and perspectives from a review of recent STAB conferences and ISSW events. Ocean. Eng. 116, 312–349.

Beck, R.F., Reed, A.M., 2001. Modern computational methods for ships in a seaway. Trans. SNAME 109, 1–51.

Belenky, V.L., Sevastianov, N.B., 2007. Stability and safety of ships: risk of capsizing - 2nd edition. Soc. Nav. Archit. Mar. Eng.

Belknap, W.F., Reed, A.M., 2010. TEMPEST: a new computationally efficient dynamic stability prediction tool. In: Proc. 11th International Ship Stability Workshop (ISSW2010), Wageningen, The Netherlands, pp. 85–197.

BLS, 2014. National Census of Fatal Occupational Injuries in 2013 (Preliminary Results). Bureau of Labor Statistics. U.S. Department of Labor.

Blume, P., 1979. Experimentelle Bestimmung von Koeffizienten der wirksamen Rolldämpfung und ihre Anwendung zur Abschätzung extremer Rollwinkel. Schiffstechnik 26, 3–23.

Bulian, G., 2004. Approximate analytical response curve for a parametrically excited highly nonlinear 1-DOF system with an application to ship roll motion prediction. Nonlinear Anal. Real World Appl. 5 (4), 725–748.

Bulian, G., 2006. Development of Analytical Nonlinear Models for Parametric Roll and Hydrostatic Restoring Variations in Regular and Irregular Waves. PhD Thesis.

Department of Naval Architecture, Ocean and Environmental Engineering, University of Trieste, Trieste, Italy.
Bulian, G., Francescutto, A., 2006. Safety and operability of fishing vessels in beam and longitudinal waves. Trans. RINA. Part B. Int. J. Small Craft Technol. 148, 1–16.
Bulian, G., Francescutto, A., 2009. Experimental results and numerical simulations on strongly non-linear rolling of multihulls in moderate beam seas. Proc. Institut. Mech. Eng. Part M J. Eng. Marit. Environ. 223 (2), 189–210.
Bulian, G., Francescutto, A., 2011. Effect of roll modelling in beam waves under multi-frequency excitation. Ocean. Eng. 38 (13), 1448–1463.
Bulian, G., Francescutto, A., 2013. Second Generation Intact Stability Criteria: on the validation of codes for direct stability assessment in the framework of an example application. Pol. Marit. Res. 20, 52–61.
Bulian, G., Francescutto, A., Sinibaldi, M., 2012. Roll motion of a ship with low metacentric height in bi-chromatic beam waves. In: Proc. 11th International Conference on the Stability of Ships and Ocean Vehicles (STAB2012), Athens, Greece, pp. 187–200.
Bulian, G., Moro, L., Brocco, E., Bresciani, F., Biot, M., Francescutto, A., 2015. Using time domain nonlinear ship motion simulations to assess safety of people and cargo onboard a container vessel. In: Proc. 16th International Congress of the International Maritime Association of the Mediterranean (IMAM 2015) - Towards Green Marine Technology and Transport, Pula, Croatia, pp. 99–110.
Bulian, G., Bresciani, F., Francescutto, A., Fucile, F., 2016. Effect of large initial ship stability on ship safety: An example study. In: Proc. 26th European Safety and Reliability Conference (ESREL2016), Glasgow, UK, pp. 2302–2309.
Cercos-Pita, J.L., Bulian, G., Pérez-Rojas, L., Francescutto, A., 2016. Coupled simulation of nonlinear ship motions and a free surface tank. Ocean. Eng. 120, 281–288.
CIAIM, 2014. Recomendaciones sobre seguridad basadas en los resultados generales de las investigaciones de seguridad marítima realizadas por la Comisión Permanente de Investigación de Accidentes e Incidentes Marítimos (CIAIM). Ref. 02/2014 – Estabilidad de los pesqueros. Comisión Permanente de Investigación de Accidentes e Incidentes Marítimos. Secretaría General de Transportes. Ministerio de Fomento. Gobierno de España, Madrid, Spain.
Cummins, W.E., 1962. The impulse response function and ship motions. Schiffstechnik 47, 101–109.
de Kat, J.O., Paulling, J.R., 1989. The simulation of ship motions and capsizing in severe seas. Trans. SNAME 97, 139–168.
DFOHS, 2014. Stability Guide for Smaller Vessels. Danish Fishermen's Occupational Health Services (DFOHS), Esbjerg, Denmark.
Dunwoody, A.B., 1989. Roll of a ship in astern seas: metacentric height spectra. J. Ship Res. 33 (3), 221–228.
E.U., 2016. Facts and Figures on the Common Fisheries Policy. Basic Statistical Data. 2016 Edition. Publications Office of the European Union, Luxembourg.
FAO, 2016a. The State of World Fisheries and Aquaculture 2016. Contributing to Food Security and Nutrition for All. Food and Agriculture Organization of the United Nations (FAO), Rome, Italy.
FAO, 2016b. FAO Yearbook. Fishery and Aquaculture Statistics. 2014. Food and Agriculture Organization of the United Nations (FAO), Rome, Italy.
FAO/ILO/IMO, 2005a. Code of Safety for Fishermen and Fishing Vessels. Part B. International Maritime Organization (IMO), London, UK.
FAO/ILO/IMO, 2005b. Voluntary Guidelines for the Design, Construction and Equipment of Small Fishing Vessels. International Maritime Organization (IMO), London, UK.
FAO/ILO/IMO, 2012. Safety Recommendations for Decked Fishing Vessels of Less than 12 Metres in Length and Undecked Fishing Vessels. Food and Agriculture Organization of the United Nations (FAO), Rome, Italy.
Francescutto, A., 2013. The evolution of the regulatory stability regime for fishing vessels. In: Proc. First International Conference “Safety and Energy Efficiency in River Transportation for a Sustainable Development of the Peruvian Amazon Region” (IDS2013), Amazonia, Iquitos, Peru, 14.1–14.18.
Francescutto, A., 2016. Intact stability criteria of ships – past, present and future. Ocean. Eng. 120, 312–317.
Francescutto, A., Contento, G., 1999. Bifurcations in ship rolling: experimental results and parameter identification technique. Ocean. Eng. 26, 1095–1123.
Francescutto, A., Bulian, G., Lugni, C., 2004. Nonlinear and stochastic aspects of parametric rolling modeling. Mar. Technol. 41 (2), 74–81.
Froude, W., 1861. On the rolling of ships. Trans. INA II, 180–229.
Greco, M., Lugni, C., 2012. 3-D seakeeping analysis with water on deck and slamming. Part 1: numerical solver. J. Fluids Struct. 33, 127–147.
Greco, M., Lugni, C., 2013. Numerical study of parametric roll on a fishing vessel. In: Proc. 32nd International Conference on Ocean, Offshore and Arctic Engineering (OMAE2013), Nantes, France, Paper OMAE2013–10690.
Grochowalski, S., Hsiung, C.C., Huang, Z.J., Cong, L.Z., 1998. Theoretical modeling of ship motions and capsizing in large and steep waves. Trans. SNAME 106, 241–267.
Gudmundsson, A., 2009. Safety Practices Related to Small Fishing Vessel Stability. Food and Agriculture Organization of the United Nations (FAO), Rome, Italy.
Gudmundsson, A., 2013. The FAO/ILO/IMO safety recommendations for decked fishing vessels of less than 12 metres in length and undecked fishing vessels – a major milestone to improve safety for small fishing vessels. In: Proc. 13th International Ship Stability Workshop (ISSW2013), Brest, France, pp. 112–120.
Himeno, Y., 1981. Prediction of Ship Roll Damping. A State of the Art. Department of Naval Architecture and Marine Engineering. The University of Michigan College of Engineering, Michigan, USA.
Hughes, M.J., Kopp, P.J., Miller, R.W., 2011. Modelling of hull lift and cross flow drag forces in large waves in a computationally efficient dynamic stability prediction tool. In: Proc. 12th International Ship Stability Workshop (ISSW2011), Washington D.C., USA.
Ikeda, Y., Himeno, Y., Tanaka, N., 1978. A Prediction Method for Ship Roll Damping. Report No.00405 of Department of Naval Architecture. University of Osaka Prefecture, Osaka, Japan.
IMO, 1993. 1993 Protocol Relating to the Torremolinos International Convention for the Safety of Fishing Vessels, 1977. International Maritime Organization (IMO), London, UK.
IMO, 2006. MSC.1/Circ.1200 - Interim Guidelines for Alternative Assessment of the Weather Criterion. International Maritime Organization (IMO), London, UK.
IMO, 2008a. International Code on Intact Stability (2008 IS Code). International Maritime Organization (IMO), London, UK.
IMO, 2008b. MSC.1/Circ.1281- Explanatory Notes to the International Code on Intact Stability. International Maritime Organization (IMO), London, UK.
IMO, 2012. Cape Town Agreement of 2012 on the Implementation of the Provisions of the Torremolinos Protocol of 1993 Relating to the Torremolinos International Convention for the Safety of Fishing Vessels, 1977. International Maritime Organization (IMO), London, UK.
ITTC, 2006. Recommended Procedure 7.5-02-07-04.3-Predicting the Occurrence and Magnitude of Parametric Rolling. In: International Towing Tank Conference (ITTC).
Jensen, O.C., Petursdottir, G., Holmen, I.M., Abrahamsen, A., Lincoln, J., 2014. A review of fatal accident incidence rate trends in fishing. Int. Marit. Health 65 (2), 47–52.
Kaplan, I.M., Kite-Powell, H.M., 2000. Safety at sea and fisheries management: fishermen's attitudes and the need for co-management. Mar. Policy 24, 493–497.
Kawahara, Y., Maekawa, K., Ikeda, Y., 2009. A simple prediction formula of roll damping of conventional cargo ships on the basis of Ikeda's method and its limitation. In: Proc. 10th International Conference on Stability of Ships and Ocean Vehicles (STAB2009), St. Petersburg, Russia, pp. 387–398.
Lincoln, J., 2010. Commercial fishing deaths - United States, 2000-2009. Morb. Mortal. Wkly. Rep. (MMWR) 59 (27), 842–845.
Liu, S., Papanikolaou, A., 2016. Prediction of parametric rolling of ships in single frequency regular and triple frequency group waves. Ocean. Eng. 120, 274–280.
Liut, D.A., Weems, K.W., Lin, W.-M., 2002. Nonlinear green water effects on ship motions and structural loads. In: Proc. 24th Symposium on Naval Hydrodynamics, Fukuoka, Japan, 2002, pp. 413–427.
MAIB, 2016. Marine Accident Investigation Branch Annual Report. 2015. Marine Accident Investigation Branch, Southampton, UK.
Mantari, J.L., Ribeiro e Silva, S., Guedes Soares, C., 2011. Intact stability of fishing vessels under combined action of fishing gear, beam waves and wind. Ocean. Eng. 38, 1989–1999.
MAPAMA, 2017. Anuario de Estadística. Ministerio De Agricultura y Pesca, Alimentación y Medio Ambiente. Avance 2016. Ministerio de Agricultura y Pesca. Alimentación y Medio Ambiente. Subdirección General de Estadística. Gobierno de España, Madrid, Spain.
Mata-Álvarez-Santullano, F., Souto-Iglesias, A., 2013. Fishing effort control policies and ship stability: analysis of a string of accidents in Spain in the period 2004–2007. Mar. Policy 40, 10–17.
Mata-Álvarez-Santullano, F., Souto-Iglesias, A., 2014. Stability, safety and operability of small fishing vessels. Ocean. Eng. 79, 81–91.
Matusiak, J., 2007. On certain types of ship responses disclosed by the two-stage approach to ship dynamics. Archives Civ. Mech. Eng. 7, 151–166.
Matusiak, J., 2010. On the non-linearities of ship's restoring and the Froude-Krylov wave load part. In: Proc. ITTC Workshop on Seakeeping - V&V for Non-linear Seakeeping Analysis. Seoul National University, Seoul, Korea, pp. 151–159.
McTaggart, K., de Kat, J.O., 2000. Capsize risk of intact frigates in irregular seas. Trans. SNAME 108, 147–177.
Meixide Vecino, A., 2015. A Economia Galega. Informe 2015. Afundación, A Coruña, Spain.
MESS, 2014. Estadística de Accidentes de Trabajo. Ministerio de Empleo y Seguridad Social. Subdirección General de Estadísticas. Gobierno de España, Madrid, Spain.
Míguez González, M., Caamaño Sobrino, P., Tedín Álvarez, R., Díaz Casás, V., Martínez López, A., López Peña, F., 2012. Fishing vessel stability assessment system. Ocean. Eng. 41, 67–78.
Míguez González, M., Diaz Casás, V., Perez Rojas, L., Pena Agras, D., Junco Ocampo, F., 2015. Investigation of the applicability of the IMO second generation intact stability criteria to fishing vessels. In: Proc. 12th International Conference on the Stability of Ships and Ocean Vehicles (STAB2015), Glasgow, UK, pp. 349–359.
Moro, L., Bulian, G., Brocco, E., Bresciani, F., Biot, M., Francescutto, A., 2015. Failure analysis of container stacks by non-linear FE simulations under non-linear inertial loads. In: Proc. 16th International Congress of the International Maritime Association of the Mediterranean (IMAM 2015) - Towards Green Marine Technology and Transport, Pula, Croatia, pp. 745–754.
Munif, A., Umeda, N., 2006. Numerical prediction on parametric roll resonance for a ship having no significant wave-induced change in hydrostatically-obtained metacentric height. Int. Shipbuild. Prog. 53 (3), 183–203.
Naciri, M., Lledo, N., 2001. Non-linear low frequency roll excitation of a rectangular barge. In: Proc. 20th International Conference on Offshore Mechanics and Arctic Engineering (OMAE'01), Rio de Janeiro, Brazil, Paper No OMAE2001/OFT-1247.
Neves, M.A.S., Rodríguez, C.A., 2006. On unstable ship motions resulting from strong non-linear coupling. Ocean. Eng. 33 (14–15), 1853–1883.
Neves, M.A.S., Rodríguez, C.A., 2009. A coupled non-linear mathematical model of parametric resonance of ships in head seas. Appl. Math. Model. 33, 2630–2645.
Ogawa, Y., 2009. A study on numerical modelling for the parametric rolling. In: Proc. 10th International Conference on Stability of Ships and Ocean Vechicles (STAB2009), St. Petersburg, Russia, pp. 533–540.
Perez Rojas, L., Perez Arribas, F., Zamora Rodríguez, R., Guerrero y Pacheco, A., 2006. On the accidents of small fishing vessels. In: Proc. 9th International Conference on the

Stability of Ships and Ocean Vehicles (STAB 2006), Rio de Janeiro, Brazil, pp. 669–676.
Peters, W., Belenky, V., Bassler, C., Spyrou, K., Umeda, N., Bulian, G., Altmayer, B., 2012. The second generation intact stability criteria: an overview of development. Trans. SNAME 119 (2011), 225–264.
Roberts, S.E., 2010. Britain's most hazardous occupation: commercial fishing. Accid. Anal. Prev. 42 (1), 44–49.
Rodríguez, C.A., Holden, C., Perez, T., Drummen, I., Neves, M.A.S., Fossen, T.I., 2007. Validation of a container ship model for parametric rolling. In: Proc. 9th International Ship Stability Workshop, Hamburg, Germany (ISSW2007), pp. 137–148.
Sadat-Hosseini, H., Stern, F., Olivieri, A., Campana, E.F., Hashimoto, H., Umeda, N., Bulian, G., Francescutto, A., 2010. Head-wave parametric rolling of a surface combatant. Ocean. Eng. 37, 859–878.
SDC 2/WP.4, 2015. Report of the Working Group (Part 1). 19 February. International Maritime Organization (IMO), London, UK.
SDC 3/WP.5, 2016. Report of the Working Group (Part 1). 21 January. International Maritime Organization (IMO), London, UK.
SDC 4/5/1, 2016. Report of the Correspondence Group (Part 1). Submitted by Japan, 11 November. International Maritime Organization (IMO), London, UK (together with SDC 4/5/1/Add.1-Add.6).
SDC 4/INF.4, 2016. Information Collected by the Correspondence Group on Intact Stability. Submitted by Japan, 9 December. International Maritime Organization (IMO), London, UK (together with SDC 4/INF.4/Add.1-Add.2).
SDC 4/WP.4, 2017. Report of the Working Group (Part 1). 16 February. International Maritime Organization (IMO), London, UK.
SLF 52/WP.1-Annex 2, 2010. Preliminary Specifications for the New Generation Intact Stability Criteria. International Maritime Organization (IMO), London, UK.
Shin, Y.S., Belenky, V.L., Lin, W.M., Weems, K.M., Engle, A.H., 2003. Nonlinear time domain simulation technology for seakeeping and wave-load analysis for modern ship design. Trans. SNAME 111, 577–583.
Somayajula, A.S., Falzarano, J., 2017. A comparative assessment of simplified models for simulating parametric roll. J. Offshore Mech. Arct. Eng. 139, 021103.
Spitzer, J.D., 1999. Dying to Fish, Living to Fish: Fishing Vessel Casualty Task Force Report. U.S. Coast Guard, Washington, DC, US.
Spyrou, K.J., Cotton, B., Gurd, B., 2002. Analytical expressions of capsize boundary for a ship with roll bias in beam waves. J. Ship Res. 46, 167–174.
Spyrou, K.J., Weems, K.M., Belenky, V., 2009. Patterns of surf-riding and broaching-to captured by advanced hydrodynamic modelling. In: Proc. 10th International Conference on Stability of Ships and Ocean Vehicles (STAB2009), St. Petersburg, Russia, pp. 331–345.
Taguchi, H., Ishida, S., Sawada, H., Minami, M., 2011. Model experiment on parametric rolling of a post-panamax containership in head waves. In: Contemporary Ideas on Ship Stability and Capsizing in Waves. Springer, Netherlands, pp. 277–294.
Tamiya, S., 1975. Capsize experiment of box shaped vessels. In: Proc. International Conference on Stability of Ships and Ocean Vehicles, Glasgow, Scotland, UK, Paper 4.2.
Tello, M., Ribeiro e Silva, S., Guedes Soares, C., 2011. Seakeeping performance of fishing vessels in irregular waves. Ocean. Eng. 38, 763–773.
Tompuri, M., Ruponen, P., Forss, M., Lindroth, D., 2014. Application of the second generation intact stabifity criteria in initial ship design. Trans. SNAME 122, 20–45.
Umeda, N., Tsukamoto, I., 2008. Simplified formula for calculating effective wave slope coefficient and its impact on ship stability assessment. In: Proc. of the 6th Osaka Colloquium on Seakeeping and Stability of Ships, Osaka, Japan, pp. 293–297.
Viggosson, G., 2009. The Icelandic Information System on Weather and Sea State, Seminar on Fishing Vessels' Crews and Stability. World Fishing Exhibition, Vigo, Spain.
Wheeler, J.D., 1969. Method for Calculating Forces Produced by Irregular Waves. Offshore Technology Conference, Dallas, Texas, US. Paper No 1006.
Wolfson Unit, 2004. MCA Research Project 530. Simplified Presentation of Fishing Vessels Stability Information. Phase 1. Final Report. Wolfson Unit. University of Southampton, Southampton, UK.
Womack, J., 2001. Exploration into the preliminary development of a weather dependent stability criteria. In: Proc. 5th International Workshop on Stability and Operational Safety of Ships (ISSW2001), Trieste, Italy, pp. 230–234.
Wellicome, J.F., 1975. An analytical study of the mechanism of capsizing. In: Proc. International Conference on Stability of Ships and Ocean Vehicles, Glasgow, Scotland, UK, Paper 3.1.
Womack, J., Johnson, B., 2003. A Guide to Fishing Vessel Stability. The Society of Naval Architects and Marine Engineers, Jersey City, NJ, US.
Wright, J.H.G., Marshfield, B.W., 1980. Ship roll response and capsize behavior in beam seas. Trans. RINA 122, 129–148.
Wu, W., McCue, L., 2008. Application of the extended Melnikov's method for single-degree-of-freedom vessel roll motion. Ocean. Eng. 35, 1739–1746.